

GRAIN-SIZE CONTROLS ON THE MORPHOLOGY AND INTERNAL GEOMETRY OF RIVER-DOMINATED DELTAS

ALEXANDER P. BURPEE,¹ RUDY L. SLINGERLAND,¹ DOUGLAS A. EDMONDS,² DANIEL PARSONS,³ JIM BEST,⁴ JAMES CEDERBERG,¹ ANDREW MCGUFFIN,¹ REBECCA CALDWELL,² AUSTIN NIJHUIS,⁵ AND JORDAN ROYCE³

¹Department of Geosciences, The Pennsylvania State University, University Park, Pennsylvania 16802, U.S.A.

²Indiana University, Department of Geological Sciences and Center for Geospatial Data Analysis, 1001 East 10th Street, Office GY425, Bloomington, Indiana 47405, U.S.A.

³Department of Geography, Environment and Earth Sciences, University of Hull, Cottingham Road, Hull HU6 7RX, U.K.

⁴Departments of Geology, Geography and Geographic Information Science, Mechanical Science and Engineering, and Ven Te Chow Hydrosystems Laboratory, University of Illinois, 133 Computer Applications Building, 605 East Springfield Avenue, Champaign, Illinois 61820, U.S.A.

⁵Department of Earth and Environmental Sciences, 140 Commonwealth Avenue, Boston College, 213 Devlin Hall, Chestnut Hill, Massachusetts 02467, U.S.A.
e-mail: sling@psu.edu

ABSTRACT: Predictions of a delta's morphology, facies, and stratigraphy are typically derived from its relative wave, tide, and river energies, with sediment type playing a lesser role. Here we test the hypothesis that, all other factors being equal, the topset of a relatively noncohesive, sandy delta will have more active distributaries, a less rugose shoreline morphology, less topographic variation in its topset, and less variability in foreset dip directions than a highly cohesive, muddy delta. As a consequence its stratigraphy will have greater clinof orm dip magnitudes and clinof orm concavity, a greater percentage of channel facies, and less rugose sand bodies than a highly cohesive, muddy delta. Nine self-formed deltas having different sediment grain sizes and critical shear stresses required for re-entrainment of mud are simulated using Deflt3D, a 2D flow and sediment-transport model. Model results indicate that sand-dominated deltas are more fan-shaped while mud-dominated deltas are more birdsfoot in planform, because the sand-dominated deltas have more active distributaries and a smaller variance of topset elevations, and thereby experience a more equitable distribution of sediment to their perimeters. This results in a larger proportion of channel facies in sand-dominated deltas, and more uniformly distributed clinof orm dip directions, steeper dips, and greater clinof orm concavity. These conclusions are consistent with data collected from the Goose River Delta, a coarse-grained fan delta prograding into Goose Bay, Labrador, Canada. A reinterpretation of the Kf-1 parasequence set of the Cretaceous Last Chance Delta, a unit of the Ferron Sandstone near Emery, Utah, USA uses Ferron grain-size data, clinof orm-dip data, clinof orm concavity, and variance of dip directions to hindcast the delta's planform. The Kf-1 Last Chance Delta is predicted to have been more like a fan delta in planform than a birdsfoot delta.

INTRODUCTION

Deltas sit at the interface between source terrains and water bodies, and their morphology and stratigraphy should reflect the influences of both domains. Traditionally, the morphologies of the world's deltas have been thought to be determined mainly by river discharge, tidal range, and wave regime, as summarized in the widely used ternary classification of deltas (Galloway 1975). Wave-dominated deltas are arcuate due to littoral drift, tide-dominated deltas have channels that are trumpet-shaped because tidal water discharges decline exponentially upstream, and river-dominated deltas are elongate with digitate shorelines because their distributaries prograde basinward. Recognizing the importance of catchment influences, Postma (1990) modified the classification of Galloway to create 12 prototype deltas that reflect the interaction of the feeder system and the basin. Orton and Reading (1993) further argued that the amount, mode of emplacement, and grain size of the sediment load delivered to a delta have a considerable effect on both the physical processes and the subsequent shape and size of the delta. They called for predictive models that better incorporate an understanding of the feeder system. Recently, Edmonds and Slingerland (2010) and Caldwell and

Edmonds (2014) used numerical experiments to quantify the effect of sediment properties on delta planform. These studies show that sediment properties, such as cohesion and the median and standard deviation of the incoming load, play a major role in determining the shapes, cumulative number of distributaries, and wetland areas of river-dominated deltas. In these experiments, elongate deltas with rugose shorelines and topographically rough floodplains are created if the incoming sediment is fine-grained and highly cohesive. Fan-like deltas with smooth shorelines and flat floodplains are created by coarser, less cohesive sediment. Other workers have lent support to the idea that sediment character strongly influences delta morphology (Jopling 1966; Falcini and Jerolmack 2010; Geleynse et al. 2011; Rowland et al. 2010; Paola et al. 2011; and Zinke et al. 2011).

The objective of the present paper is to further explore the role that sediment type plays in delta formation by better quantifying the functional relationships among sediment type, deltaic morphology, and delta facies and stratigraphy. Unlike previous research (Edmonds and Slingerland 2010; Geleynse et al. 2011; and Caldwell and Edmonds 2014), which has focused on the morphological effects of sediment properties,

we include delta facies and stratal architecture because these are more readily observable in ancient sediments than delta planform and allow us to test model predictions with observations in the rock record. Specifically, we conjecture that in the absence of appreciable waves and tides: 1) a relatively noncohesive, sandy delta will have more active distributaries, a less rugose shoreline morphology, less topographic variation in its topset, and less variability in foreset dip directions than a highly cohesive, muddy delta; and 2) the stratigraphy of this sandy delta will have greater clinoform dip magnitudes and clinoform concavity, a greater percentage of channel facies, and less rugose sand bodies than a highly cohesive, muddy delta. If proven, these conjectures should allow prediction of deltaic planform and stratigraphy from knowledge of the grain sizes composing a delta.

The present research adopts a threefold approach: 1) we create a suite of nine numerical experiments using Delft3D to predict delta morphology, facies, and stratigraphy as a function of sediment size. Our modeling setup is similar to that of Caldwell and Edmonds (2014) in that we model a phi-normal grain-size distribution, thereby extending the more simplified approaches of Edmonds and Slingerland (2010) and Geleynse et al. (2011); 2) we test the model predictions using geomorphological and stratigraphic field observations of the modern Goose River Delta, Labrador, Canada; and 3) we reinterpret a parasequence set in an ancient delta, the Last Chance Delta of the Ferron Sandstone, Utah, USA in light of these results. We aim to test if there are predictable relationships between delta planform and clinoform morphology, facies partitioning, and sandstone reservoir geometry for various sediment grain sizes.

Background

Current research into the conditions necessary to produce a particular delta morphology and stratigraphy remains limited, although Giosan et al. (2005), Syvitski (2006), Syvitski and Saito (2007), and Syvitski (2008) provide statistical relationships of delta morphologies as a function of fluvial variables such as water discharge. Most current depositional models of deltas assume that their internal facies distribution and stratigraphic architecture are strongly dependent on the origin of the deltaic planform morphology (Galloway 1975; Bhattacharya 2006) and that delta sand-body geometries can be classified based on the relative magnitudes of river, wave, and tidal energies (Galloway 1975). While this scheme may be applicable in some cases, several studies have recognized that the internal stratigraphy of a delta may differ from that expected from these planform-dependent facies models. For example, deltas classified as wave-dominated based on plan-view morphology may have a facies architecture that is more fluvially influenced (Rodriguez et al. 2000; Fielding et al. 2005) or tidally influenced (Lambiasi et al. 2003). A possible explanation for this discrepancy was given by Postma (1990), Orton and Reading (1993), and Edmonds and Slingerland (2010), who proposed that a variety of delta morphologies bearing resemblance to wave-, tide-, and river-dominated morphologies can be created by changing the relative cohesion of the deltaic sediment.

While it is generally accepted that noncohesive deltas are fan-like, constructed by more simultaneously active distributaries, and their stratigraphy is characterized by angle-of-repose foresets (McPherson et al. 1987; Postma 1990), and that finer-grained deltas are constructed by fewer simultaneously active distributaries, it is challenging to tease out cause and effect. Postma (1990) and Orton and Reading (1993) hypothesized that the steepness of a delta-front clinoform and coastal plain increases with increasing grain size, and that these conditions predispose coarse-grained systems to be more susceptible to strong wave influence and less susceptible to tidal influence. This susceptibility arises because coarse-grained foresets are steeper, thereby allowing waves to impinge more energetically on the delta front. Their coastal plains are also steeper, thereby restricting tidal influence.

The dependency of clinoform geometry upon sediment properties and delta morphology is also poorly understood. A clinoform is a chronostratigraphic surface cutting obliquely through a heterolithic, coarsening-upward succession, such as commonly observed as a single basinward-dipping seismic reflector, whereas the term clinothem defines the deposits separated by clinoforms (Mitchum et al. 1977). We argue that clinoform geometry is a function of four semi-independent variables: i) the rate of creation of accommodation space, ii) the sediment caliber of the delta, iii) the type of distributive processes on the delta topset, and iv) the stage of delta development. Research exploring the relative contributions of these independent variables to clinoform geometry has used theory (Driscoll and Karner 1999; Kostic and Parker 2003a, 2003b), physical experiments (Paola et al. 2001; Pratson et al. 2004; Niedoroda et al. 2005), and observations of many modern clinothems around the world (Kuehl et al. 1986; Nittrouer et al. 1986; Nittrouer et al. 1995), although the latter are distal, subaqueous, muddy-prodelta shelf clinoforms. But to date, there has been no systematic inventory of deltaic stratigraphy as a function of sediment type while holding all other external forcing factors constant. This paper presents a first step to addressing this gap in knowledge.

QUANTITATIVE ATTRIBUTES OF DELTA FORM AND STRATIGRAPHY

We define three metrics to quantify differences in delta topsets: 1) the number of active distributaries (N), 2) shoreline rugosity (R), and 3) topset roughness (T), and four metrics to quantify delta stratigraphy: 1) average clinoform dip magnitude (α), 2) a clinoform dip azimuth statistic (measured as the sum of the deviations of clinoform dip azimuths from a theoretical uniform circular distribution) (U^2), (3) average clinoform concavity (C), and 4) facies proportion (F). Our investigation is conceived as a multiple-regression problem where this set of variables is a function of the independent variables sediment grain size (D_{50}) and cohesion (K):

$$(N, R, T, \alpha, U^2, C, F) = f(D_{50}, K) \quad (1)$$

The number of active distributaries (N) is defined as the time-averaged number of distributaries that deliver enough sediment to the delta shoreline to cause morphologic change over the time interval of averaging. Distributaries that pass water and sediment, but do not participate in morphodynamic evolution at the shoreline, are not counted. This variable is easy to measure in model and modern deltas by taking temporal snapshots either numerically or from aerial photographs. In ancient deltas, this variable could be quantified by defining the proportion of channel facies in the topset, but this is not developed further herein.

Shoreline rugosity (R) is used as a measure to quantify the planform difference between fan and birdsfoot deltas. There is no widely accepted method for quantifying delta shoreline rugosity, and herein we use the quotient

$$R = \frac{P^2}{4\pi A} \quad (2)$$

where P is the perimeter [m] and A is the area [m²] of a delta as defined below. Notice that R is dimensionless and is devised such that a circle has the value of unity and a half-circle a value of $(\pi+2)^2/2\pi^2 \approx 1.34$. Highly rugose, complex shorelines with shapes that deviate from a half-circle have R values higher than 1.34, while low rugosity, uniform shorelines that approximate a fan should approach $R = 1.34$. The rugosity of numerical and modern deltas is measured by fitting a polygon to the delta topset and computing the area and perimeter of the polygon. Shoreline

points defining the wetted perimeter are selected using the open-angle method proposed by Shaw et al. (2008) with a threshold angle of 25° . A straight line connects the two landward end points of the shoreline. In the numerical deltas, rugosity is computed at equally spaced time intervals during delta growth and then averaged. The question arises of whether shoreline length is fractal. Herein we assume not, because Wolinsky et al. (2010) showed that shorelines are nonfractal while networks are fractal. Therefore our metric should be insensitive to window size.

The roughness of a delta topset (T) is defined as the standard deviation of the topset topography greater than an elevation of -0.1 m. We use this value rather than sea level because Delft3D considers waters shallower than 0.1 m as dry land. Delta topset roughness is viewed as an important variable because Edmonds and Slingerland (2010) conjectured that it indirectly controls the frequency of distributary avulsions, and therefore determines the distribution of sediment along the delta perimeter. For numerical and modern deltas, the topset elevations were measured every 25 m along a randomly chosen strike line. F-tests of the measurements of topset roughness from random line orientations indicate that as the position of a strike line on the delta becomes more proximal or distal, the average and maximum elevations change, but the standard deviation does not vary appreciably.

The magnitude of the clinoform dip (α) is defined as the angle between the clinoform and a horizontal line, and can be either true or apparent. Measurements were collected using three methods: the two-point, concavity, and bathymetric methods. The two-point method calculates the slope angle between the rollover point of a delta foreset and its toe, regardless of whether this is a true or apparent dip. The rollover point is defined as the inflection point between the convex and concave portions of a clinoform, or when the rollover point has been eroded, it is defined as the highest elevation on the clinoform. The clinoform toe is defined as the point where bedding surfaces become so condensed that it is no longer possible to follow an individual clinoform. The concavity method defines at least five points in x - y - z space along a clinoform surface between the rollover point and clinoform toe and averages the slopes measured between adjacent points, yielding an apparent dip. Lastly, the bathymetric method uses the 3D bathymetry of the foreset to calculate the average downslope angle of a delta foreset from the clinoform rollover to the toe, and thus measures the true magnitude of clinoform dips.

The foreset dip azimuth statistic (U^2) measures the sum of the deviations of clinoform dip azimuths from a theoretical uniform circular distribution, and is given by

$$U^2 = \sum_{i=1}^N \left[U_i - \bar{U} - \frac{i-1/2}{N} + \frac{1}{2} \right]^2 + \frac{1}{12N} \quad (3)$$

where U_i are the observed azimuthal data, \bar{U} is their simple mean, and N is the number of observations (Jones 2006). This statistic is a potentially informative measure because it should reflect delta planform shape, and in ancient deltas it provides information concerning the geometry of the delta paleoshoreline. For example, fan delta fronts that develop self similarly with a radial spread of 180° possess small values of U^2 that approach zero, whereas a birdsfoot delta with multiple distributaries growing to the north and many dips clustering due east and west has a U^2 value greater than 100. The foreset dip azimuth statistic can most readily be measured in numerical or modern deltas where the entire foreset is known; in ancient deltas it can be measured from high-quality 3D seismic data and 3D outcrops.

Cliniform concavity (C) is a measure of the rate of change of slope along a clinoform surface from the rollover point to the toe, and is valuable for connecting stratigraphy to depositional processes. Cliniform concavity should depend upon the relative proportions of grains

deposited on the delta front to clinoform toe from bed-load or suspended-load transport. Rapid bedload sedimentation at the rollover should produce Gilbert-delta-type planar foresets (cf. Soria et al. 2003). Herein, concavity is measured by fitting a second-order polynomial to a minimum of five equally spaced points along a geo-referenced clinoform and taking its second derivative. Thus, if the polynomial is of the form

$$y = ax^2 + bx + c$$

$$\text{then} \quad (4)$$

$$\frac{d^2y}{dx^2} = 2a$$

and the concavity is $2a$. Cliniform concavity can be measured in outcrop and seismic cross sections in addition to modern delta bathymetry, but because lobes prograde in various directions, the traces of clinoforms will record both apparent and true dips. To determine the influence of this mixing on the concavity measurement, concavities were calculated along four random cross sections of a single numerically modeled delta, resulting in concavities of 3.51×10^{-6} , 3.52×10^{-6} , 3.25×10^{-6} , and 4.10×10^{-6} . This variation (0.85×10^{-6}) is small compared to the range of concavities among the nine deltas (9.14×10^{-7} to 3.87×10^{-4}).

The proportion of distributary-channel and foreset facies (F) is an important attribute of delta stratigraphy, and is thought to reflect the mobility and number of distributaries as well as the basin geometry. It is quantified herein by computing the areal proportions of channel and foreset facies in vertical transects through the model deltas. On both a standard dip and strike panel, the channel and foreset facies were identified by bedding geometry and by comparison with delta bathymetry at various stages of delta growth. The cumulative cross sectional area of all channel facies was then divided by the total cross sectional area of the panel to obtain the proportion of the cross section occupied by channel facies. The measurements for the dip and strike line were then averaged.

NUMERICAL EXPERIMENTS

In order to gain insight into how grain size controls stratigraphy, we first conduct a modeling experiment that allows the morphological features to be unambiguously linked to their stratigraphic expression. Nine experimental deltas are simulated using Delft3D (v. 4.00.01), a numerical fluid-flow and sediment-transport model (Lesser et al. 2004; Marciano et al. 2005). These Delft3D simulations are not meant to be facsimiles of the Goose River and the Last Chance delta of the Ferron Sandstone, but rather statistical representations of similar deltas in the same general part of parameter space. Previous work has shown that Delft3D predicts the basic spatial and temporal structure of delta islands and channels correctly (Wolinsky et al. 2010; Edmonds et al. 2011b), which gives us confidence in the predicted quantitative attributes described in the previous sections. These studies demonstrated that Delft3D simulations bear similarity to real deltas in terms of their temporal growth patterns, the fractality and structure of the channel network, and the distribution of planform shapes of sedimentary bodies.

Model computations solve the depth-averaged, nonlinear, shallow-water equations, and sediment transport and conservation equations. The contribution of sub-grid-scale turbulence to the horizontal viscosity coefficient is modeled using the horizontal large eddy simulation technique (HLES) presented in Uittenbogaard and van Vossen (2004). The solution domain consists of 300×225 computational cells, each of which is $25 \text{ m} \times 25 \text{ m}$ in the horizontal (Table 1). The upper surface of each cell in the vertical is defined by the water (or land) surface and is dynamic. The sediment-water interface also is dynamic, moving up or

TABLE 1.—User-defined model parameters for runs in this study.

User-Defined Model Parameter	Value	Units
Grid size	302 × 227	cells
Cell size	25 × 25	m
Initial basin bed slope	0.000375	—
Initial channel dimensions (width×depth)	250 × 2.5	m
Upstream open boundary: incoming water discharge	1000	m ³ s ⁻¹
Downstream open boundary: constant water surface elevation	0	m
Initial sediment layer thickness at bed	20	m
Subsurface stratigraphy bed layer thickness	0.1	m
Number of subsurface stratigraphy bed layers	100	—
Time step	0.1	min
Morphological scale factor	175	—
Spin-up interval before morphological updating begins	1440	min
Spatially constant Chézy value for hydrodynamic roughness	45	m ^{1/2} s ⁻¹
Background horizontal eddy viscosity and diffusivity (added to subgrid horizontal large eddy simulation)	0.001	m ² s ⁻¹
Factor for erosion of adjacent dry cells	0.25	—
Number of sediment fractions	6	—
Cohesive sediment critical shear stress for erosion ($\tau_{ce(C)}$)	0.25, 1.75, or 3.25	Nm ⁻²
Cohesive sediment critical shear stress for deposition ($\tau_{cd(C)}$)	1000	Nm ⁻²

down depending upon the amount of sediment erosion or deposition. Below the sediment–water interface lie one hundred 0.2-m-thick cells containing sediment whose grain-size distribution consists of either the initial bed size distribution, or the grain-size distribution of sediment that has been deposited there. A time step of 6 s is used in order to preserve numerical stability. We reduce the computation time by using a morphologic scale factor of 175 (see Ranasinghe et al. 2011 for a discussion of this technique). A rectangular trunk stream 250 m wide and having an initial depth of 2.5 m flows seaward into a basin through a 500-meter-wide sandy shoreline trending perpendicular to the trunk stream. Water and sediment discharges at the boundary are kept steady at 1000 m³ s⁻¹ and 0.1 kg s⁻¹, respectively. Open boundaries on the other three sides of the basin allow both water and sediment to pass and are defined with a constant water elevation equal to zero. The basin possesses no waves, tides, Coriolis acceleration, or temperature or salinity variations, thereby precluding hyperpycnal flows. The initial basin bathymetry for each numerical experiment slopes seaward from 0 m to 3.5 m, and the basin depth is shallow to reduce simulation times. Each simulation represents 41 years of delta growth, assuming that bankfull flows occur for 14 days a year. This interval is sufficient for multiple channel lobes to form. Thus the model deltas are representative of natural deltas prograding into shallow, fetch-limited lakes and marine basins, such as Wax Lake Delta, Louisiana, USA.

In the model, sediments are categorized as either cohesive or noncohesive. Noncohesive sediments, defined as grain diameters greater than 64 μm (i.e., sand and coarser), may travel as suspended or bedload material as governed by the van Rijn equation (van Rijn 1993) with erosion and deposition determined from the Shields curve. Cohesive sediments, finer than 64 μm , are treated as suspended material and governed by the Partheniades-Krone formula (Partheniades 1965) with erosion and deposition calculated as source and sink terms in an advection–diffusion equation. Erosion of cohesive sediment occurs when the bed shear stress (τ_b) exceeds the critical shear stress required for re-erosion of cohesive sediments (τ_{cre}), with the latter threshold being set by the user.

Experimental Design

Three ratios of noncohesive to cohesive sediment (90:10, 50:50, 10:90) and three critical shear stresses for erosion of cohesive sediment (0.25,

1.75, 3.25 N m⁻²) are used in combination to create nine deltas. This sediment consists of three noncohesive and three cohesive size classes with grain diameters of 300, 150, 80, 32, 13, and 7.5 μm . The six sediment fractions compose an approximate phi-normal distribution, with the smallest and largest size fractions always constituting the smallest proportion of the total sediment load. Deltas are fed a 90%, 50%, or 10% sand mixture for which the median grain diameters are 177, 74, and 22 μm , respectively. These are called sand-dominated, sand-mixed, and mud-dominated, respectively, while deltas experiencing a critical shear stress required for erosion of cohesive sediments (τ_{cre}) of 0.25, 1.75, and 3.25 N m⁻² are called low-cohesion, medium-cohesion, and high-cohesion deltas, respectively. While a Monte Carlo approach, in which boundary and initial conditions are statistically varied, would have been preferable, the computational time needed for deterministic runs of this type precluded this approach at present.

Probably only short, steep, arid rivers approach 90% sand delivery to their sedimentary basins, and so the sediment flux of 90% used in this study requires some explanation. This study, together with those by Edmonds and Slingerland (2010) and Caldwell and Edmonds (2014), indicate that it is the proportion of noncohesive to cohesive sediment composing the delta that determines the morphology of a delta. An example of a delta whose depositional sand/mud ratio is larger than the sediment being fed from upstream is the Wax Lake delta, where a sediment feed of 17% sand produces a delta that is 67% sand (Shaw et al. 2013). We attribute this mismatch to washload bypassing and some resuspension by small waves in Atchafalaya Bay. By our selection of the critical shear stresses for mud erosion and deposition and by ignoring waves, we have allowed the mud fraction of the sediment feed to be deposited in the delta and exert a morphodynamic influence, rather than bypass the delta. Therefore, to match the actual sand content of natural deltas, we must specify a higher than average sand proportion in the sediment fed to the delta. Also, the sand/mud ratios transported by modern rivers are very poorly quantified. They are usually estimated from bedload/suspended load ratios, and that is an inaccurate indicator because much of the sand fraction is transported as suspended load. Probably a better estimate of the global delivery of sand and mud to sedimentary basins is given by the proportions of sandstone (22%) and mudrock (63%) in all extant sedimentary rocks (Prothero and Schwab 2004). But those proportions include the big, continent-draining rivers

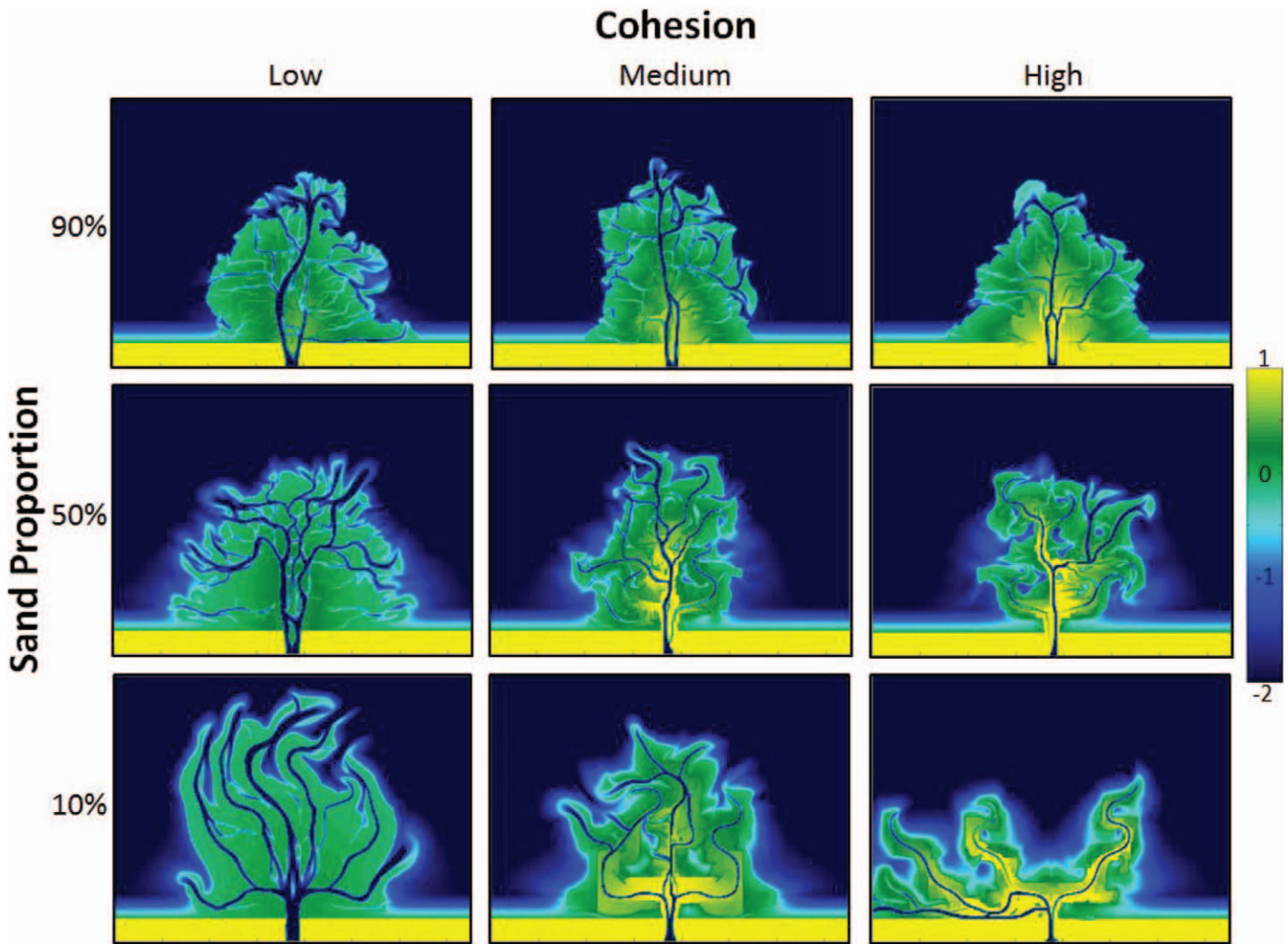


FIG. 1.—Topography of deltas computed by Delft3D under varying sediment types (all other boundary conditions held constant). Scale bar on right shows elevations from +1 to -2 m; areas in blue are all shallower than -2 m. **A–C**) The sand-dominated deltas (upper row) tend to have a fan shape over the three degrees of cohesion, but the mouth-bar size appears to decrease with increasing cohesion. **D–F**) The sand–mud mixed (middle row) and **G–I**) mud-dominated deltas (bottom row) develop irregular complex shorelines with increasing cohesion. Topset elevations for all deltas increase with increasing cohesion.

that are mud-dominated, indicating to us that orogenic rivers draining into epicontinental seas would transport sand in proportions higher than 22%.

Available bed material in each model run consists of 20 m of evenly mixed sediment equivalent to the grain size proportions of the incoming sediment feed. All particles have a density of $2,650 \text{ kg m}^{-3}$. Dry bed densities (bulk densities of sediment assuming air occupies all pore spaces) are 500 kg m^{-3} for cohesive sediments and 1600 kg m^{-3} for noncohesive sediments. The model precludes deposition of sediment in water depths shallower than 0.1 m to eliminate computational instabilities due to supercritical flow. To simulate channel-widening into dry cells, 25% of the sediment in a cell that experiences erosion is taken from the adjacent dry cell. A complete set of files for reproducing our delta *D* in Figure 1 is included in the SEPM data repository (see Supplemental Material) as Run 1. The files, which can be read using any text editor, give the values of all variables and parameters. Other deltas in Figure 1 can be reproduced by varying the sand proportion and critical shear stresses for re-erosion of cohesive sediments given in Table 2.

The model stratigraphy is constructed using the chronostratigraphic surfaces and sediment grain size of each model layer. The

chronostratigraphic surfaces are generated from bed-elevation data recorded at evenly spaced time increments during delta growth. Grain sizes are recorded in 100 subsurface sediment layers, each 0.2 m thick, that store the D_{50} grain size in each layer in each cell. The measurements of the morphology and stratigraphy in each delta are made after an identical volume of sediment has passed into the basin.

Results

The numerical experiments produced nine self-formed deltas constructed by the three sediment types and three critical shear stresses for re-erosion of cohesive sediment (Figs. 1, 2; Table 2). The nine deltas show different shoreline shapes and bathymetries for each combination of sediment load and cohesion, with the greatest difference occurring between the sand-dominated, low-cohesion delta and the mud-dominated, high-cohesion delta (Fig. 1A and 1I, respectively). Their stratigraphies also differ (Fig. 2) such that sandy deltas possess more steeply-dipping clinofolds and flatter tops than muddy deltas. All of the deltas preserve a sand fraction that is 5 to 10% greater than the sand fraction of the

TABLE 2.—Morphometric and stratigraphic attributes of the nine numerically modeled deltas.

ID	Sand (%)	D ₅₀ (μm)	τ _{cre} (Pa)	N	R	T (m)	U ² (°)	α (°)	C	F (Channel)	Reservoir Rugosity
A	90.00	177	0.25	12.00	3.45	0.11	17	0.92	0.00029	70.00	2.33
B	90.00	177	1.75	11.00	3.45	0.15	15	0.92	0.00034	69.10	1.89
C	90.00	177	3.25	10.00	3.70	0.24	45	1.22	0.00039	62.10	2.50
D	50.00	74	0.25	11.00	5.00	0.09	102	0.12	0.00000	60.80	3.70
E	50.00	74	1.75	10.00	3.45	0.33	104	0.16	0.00000	53.50	3.45
F	50.00	74	3.25	7.00	3.70	0.43	62	0.23	0.00000	53.00	4.17
G	10.00	22	0.25	6.00	5.00	0.04	107	0.11	0.00000	52.50	10.00
H	10.00	22	1.75	3.00	3.57	0.23	131	0.10	0.00000	46.70	11.11
I	10.00	22	3.25	4.00	5.56	0.33	176	0.07	0.00000	29.10	14.29
GRD	~90	~150	low	14	2.1	0.11	16	4	0.00009	n/a	n/a
LCD	~80	~125	med	n/a	n/a	n/a	1.1	7.40	0.01300	12.1	n/a

Parameters for each numerical delta are given with their corresponding topset and stratigraphic attribute values. Letters provided for “ID” correspond to those given in Figure 1. GRD, Goose River Delta; LCD, Cretaceous Last Chance Delta; Sand (%), proportion of sand delivered to the delta (unitless); D₅₀, median grain size of the sediment entering the basin; τ_{cre}, critical shear stress required for re-erosion of cohesive sediment (N m⁻²). Topset variables (see text for definitions): N, number of active distributaries (unitless); R, shoreline rugosity (dimensionless); T, topset roughness (m); U², foreset dip azimuth statistic (degrees²). Stratigraphic variables: α, clinoform dip magnitude (degrees); C, clinoform concavity (unitless); F (Channel), channel facies proportion (dimensionless); n/a denotes variables not measured.

sediment feed, because even without wave resuspension, some of the mud bypasses the delta topset and is deposited in the bottomset.

We measured the variables on one numerical delta at various stages of its evolution to test for their stationarity. Results showed that after an initial period of establishment, the distributary network stabilized to a mean number of channels, as did all other measurement variables. Therefore we measured each of our numerical deltas after dynamic equilibrium had been obtained. The only exceptions were rugosity, which was computed at equally spaced time intervals during delta growth and then averaged, and the proportion of distributary channel and foreset facies (F), which is an average for the whole delta, excluding its start-up deposits. Our approach is similar to that of Caldwell and Edmonds (2014), who noted in similar modeling runs (cf. their fig. 7) that deltas also attained a dynamic equilibrium after an initial establishment period.

Delta Topset Characteristics.—The number of active distributaries on each delta topset increases from 3 to 12 with an increasing proportion of sand delivered to the delta (Fig. 3A; Table 2). In general, sand-dominated deltas possess a greater number of active distributaries than mud-dominated deltas, and more bifurcations. The distributary channels are generally consistent with the hydraulic geometry expected for a river passing 1000 m³ s⁻¹, being only a meter or two deeper. These distributary channels cut completely through the delta foresets because in these model simulations the deltas build into a shallow basin. The model results mirror the case of Wax Lake Delta, where channels 6–7 m deep cut below the delta deposits into pre-delta bay muds. If the first distributary bifurcation is termed first order, and successive bifurcations along a distributary are assigned a successively increasing order, then fine-grained deltas are of order one or two, and coarse-grained deltas are of order five or more. Sand-dominated deltas also tend to have the smoothest shorelines (Fig. 3B). The topset roughness (variance of elevations above -0.1 m elevation) shows no clear relationship with sand percentage, but increases monotonically with sediment cohesion (Fig. 3C).

Delta Stratigraphy.—Clinoform dips for the modeled deltas increase on average from 0.09° for mud-dominated deltas to 1° for sand-dominated deltas (Figs. 2, 3D; Table 2). The delta foreset dip-azimuth statistic systematically decreases with increasing sand proportion delivered to the delta (Fig. 3E), and mud-dominated deltas have the highest deviation from a uniform circular distribution in dip directions. Dip directions also deviate less from a uniform distribution as the number of channels

increases (Fig. 4). Clinoform concavity measured along a stratigraphic dip section also increases with increasing proportion of sand delivered to the delta (Fig. 3F). Cohesion does not systematically control clinoform concavity, likely because clinoforms are depositional, not erosional, features. The average proportion of channel facies is greater, with an increasing proportion of sand delivered to the delta and with decreasing cohesion (Fig. 3G). The proportion of channel facies also statistically increases with the number of distributaries (Fig. 5). Finally, sand-dominated deltas create larger coherent sand bodies in which the isolith area increases with decreasing cohesion (Fig. 6), with the end member being a mud-dominated delta containing shoestring sands. The rugosity of this potential reservoir (Table 2) becomes more digitate with increasing mud proportion and cohesion, similar to the delta shoreline.

Discussion

The morphology and internal stratigraphy of the topsets of these nine numerically modeled deltas can be understood in terms of delta growth processes. Muddy deltas are fed by fewer distributaries because the higher cohesion of the topset sediment stabilizes the banks, as found by Edmonds and Slingerland (2010), and also because the low gradient increases the avulsion time scale (Caldwell and Edmonds 2014). With stabilized banks, the levees grow higher, thus producing greater topset roughness. These levees are also more resistant to erosion and avulsion, thereby promoting progradation of channel mouths. Consequently, the delta perimeter receives sediment at fewer points, resulting in a more rugose shoreline. Deltas on the Gulf of Mexico coast are good examples of this process because their distributaries erode into stiff prodelta muds (Edmonds et al. 2011b, Shaw et al. 2013), which in the case of the Mississippi Delta has been argued to prohibit lateral migration of distributaries, thereby creating a highly rugose shoreline (Coleman and Prior 1982). These results also are consistent with the qualitative conclusion of Olariu and Bhattacharya (2006), who determined that “the number of terminal distributaries controls ... the overall shape of the shoreline.” Olariu and Bhattacharya (2006) were specifically referring to “terminal distributaries,” which they defined as either subaqueous or subaerial distributaries around river mouth bars, but if the number of subaerial upstream distributaries is greater, then the number of terminal distributaries also would be increased.

The stratigraphy of these nine experimental deltas is controlled by four principal factors: i) the number of distributaries, ii) the distance seaward at which mouth bars form, iii) the probability that the bifurcation around

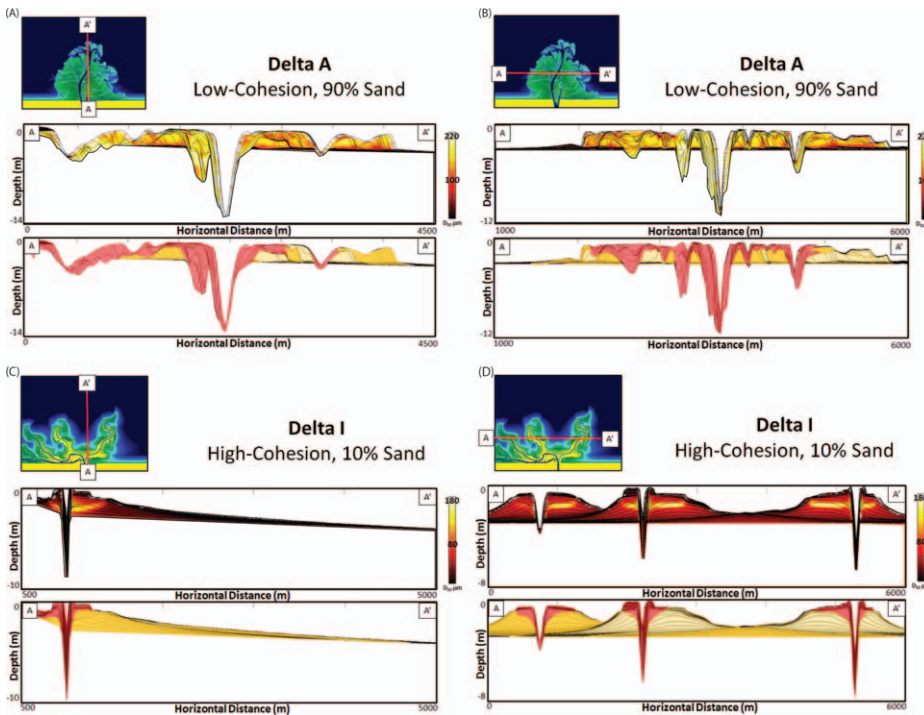


FIG. 2.—Predicted stratigraphy along A, C) dip and B, D) strike lines for deltas A and I in Figure 1. Upper panel of each row shows D_{50} (color bar on right in μm); black lines are clinoforms. Notice the coarsening-upward yellow portions, the clinoform dips and shapes, and the fine-grained clinoform toes. Bottom panel shows fluvial facies in pink; foreset autogenic parasequences composed of different delta lobes are indicated by different shades of orange. In dip lines parasequences change from older to younger from left to right; notice the onlap of some younger parasequences onto older.

a mouth bar is stable with two active channels, and iv) the mechanics of grain dispersal in the expanding turbulent jets. All of these factors are a function of grain size (Edmonds and Slingerland 2007, 2008, 2010; Caldwell and Edmonds 2014). Clinoform dips increase with grain size because coarse-grained bedload transport is delivered to the clinoform rollover whilst finer-grained suspended load is transported seaward in the expanding jet, settling out on the clinoform toe. These results pertain only to deltas that do not produce muddy, hyperpycnal turbidity currents. As Kostic and Parker (2003a, b) showed in flume experiments, a muddy turbidity current overriding a sandy foreset reduces the foreset angle by 20%. When scaled to field dimensions, this angle can be reduced to as low as 1° by this mechanism. But the process of angle reduction is self-limiting because successively lower foreset angles push the plunge point successively farther out, so mitigating further reduction in foreset angle. Dip directions also deviate less from a uniform distribution as grain size increases, because a larger number of channels distribute sediment more evenly around the delta perimeter, thereby reducing the shoreline rugosity (Fig. 4). Clinoform concavity increases with increasing proportion of sand because the dip magnitudes at the clinoform rollover increase due to a greater proportion of bedload transport there, whilst the clinoform toe continues to approach horizontal asymptotically. The proportion of channel facies preserved in cross section becomes larger with increasing grain size because the number of active distributaries increases with grain size and the proportion of channel facies correlates with the number of distributaries. Finally, sand-body geometry is a function of the number of distributaries (Olariu and Bhattacharya 2006), and the number of distributaries decreases with decreasing grain size. Therefore, finer-grained deltas possess more rugose or digitate sand bodies.

TESTING MODEL PREDICTIONS

Goose River Delta

As a test of these predictions, we collected morphological and stratigraphic data from the Goose River Delta, an unvegetated, fan-shaped

delta prograding into Goose Bay at the western end of Lake Melville fjord in Labrador, Canada (Fig. 7). The delta is fed by the Goose River, a small, ungauged Arctic river draining 3436 km^2 of the Labrador Plateau in a region that receives between 750 mm and 1000 mm mean annual precipitation (Anonymous 2001). Thus, its mean annual discharge is estimated to be $100 \text{ m}^3 \text{ s}^{-1}$, although spot measurements from 1948 to 1952 (Coachman 1953) show that its monthly discharge is highly variable from $5 \text{ m}^3 \text{ s}^{-1}$ in March (under ice) to $532 \text{ m}^3 \text{ s}^{-1}$ in May. Its sediment load and the influence of ice and ice-rafting on that load are unknown. Cut banks up to 12 m high expose topsets and foresets of older delta lobes consisting of a mixture of quartz, feldspar, and heavy minerals derived from plutonic and metamorphic rocks of the Canadian Shield (Wardle et al. 1986). Thin to thick sand beds are separated by thin silt-clay drapes constituting less than 10 percent of the whole. Sand grain sizes range from lower fine at the bottom to upper coarse in the topset beds. Sediment samples collected from these topset and foreset facies, and from bottom grabs down the modern delta front, were subjected to laser particle-size analysis. The resulting sample median diameters were then weighted by measuring the vertical distance between samples and interpolating to approximate the change in grain size moving down the delta front. The interpolated, weighted values were then averaged to obtain an average grain size for the Goose River Delta of $150 \mu\text{m}$, with grains ranging from $\sim 10 \text{ cm}$ diameter cobbles to $<20 \mu\text{m}$ clays.

The Goose River Delta contains at least three inactive lobes, the youngest of which is indicated in Figure 7B, and two active lobes. The delta presently is prograding into a bay that is microtidal (0.5 m amplitude) (Vilks et al. 1987) and has a surface salinity of no more than 10 ppm (Vilks and Mudie 1983). Prevailing winds during ice-free conditions blow offshore so that the delta experiences only minor wave influence. Consequently, tides, buoyancy effects, and waves are minimal, making the Goose River Delta a reasonable test case for the model predictions. However, it is important to note that postglacial rebound has subjected the Goose River to an average relative base-level

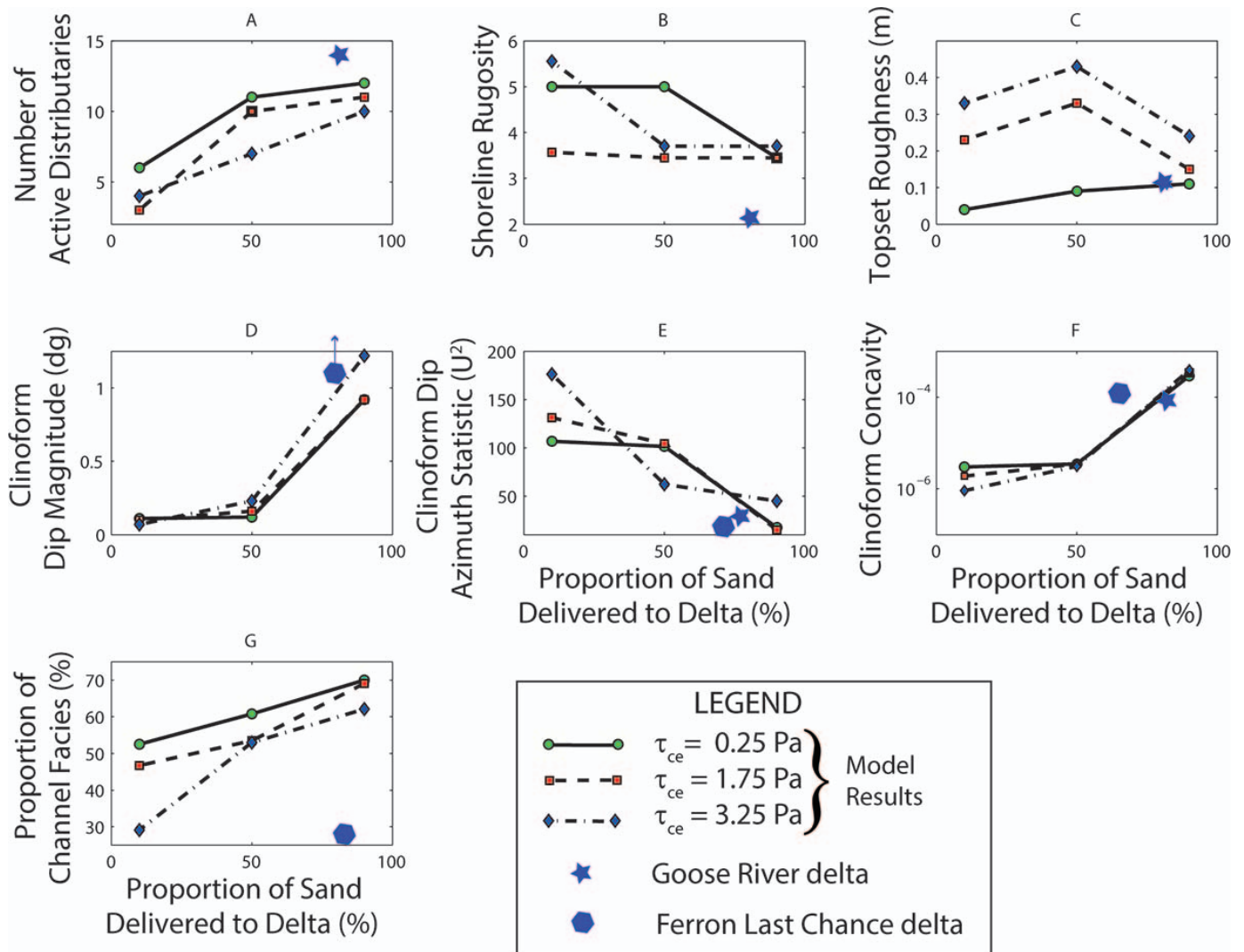


FIG. 3.—Predictions of various delta metrics from Delft3D. **A)** Number of active distributaries increases with increasing proportion of sand delivered to the delta. The number of distributaries also increases with decreasing cohesion, except for mud-dominated deltas. **B)** Rugosity values generally decrease with increasing proportion of sand delivered to a delta. The high-cohesion, mud-dominated delta has the greatest rugosity and the low-cohesion, sand-dominated delta has the smallest rugosity. **C)** Roughness of delta topset (standard deviation of elevations greater than -0.1 m) increases with increasing cohesion. Sand-mixed deltas develop the roughest topsets. **D)** Foreset dip magnitudes increase with increasing proportion of sand delivered to a delta. Cohesion does not participate strongly in determining clinoform dip magnitude because dip is set by deposition not erosion. **E)** Delta foreset dip-azimuth uniformity decreases with increasing proportion of sand delivered to the delta. The foreset with the largest sum of deviations from a uniform circular distribution is the high-cohesion, mud-dominated delta. **F)** Clinoform concavity increases with increasing proportion of sand delivered to the delta. Cohesion does not seem to control clinoform concavity. **G)** Proportion of channel facies relative to foreset facies increases with increasing proportion of sand delivered to the delta and with decreasing cohesion.

fall of ~ 3 to 5 mm yr^{-1} (Clark and Fitzhugh 1992; Liverman 1997). Furthermore, since the retreat of the Laurentide ice sheet about 7500 yr BP (Vilks and Mudie 1983), the Goose River Delta has prograded over an irregular fjord bathymetry with water depth at the toe of the foreset being approximately 30 m. Our model runs do not account for this base-level fall and irregular basal boundary condition. A subsequent unpublished MSc thesis by one of the authors (Cederberg 2014) investigates the effect of basin depth and base-level fall on delta planform through Delft3D modeling. Increased basin depth increases the avulsion period, which results in more rugose shorelines and more variability in foreset dip directions. This is also generally consistent with physical experiments (Carlson et al. 2013). Higher rates of base-level fall result in more elongate deltas with greater topset roughnesses caused by downstepping lobes. The conclusions drawn below are tempered by these considerations.

Methods

The number of active distributaries on the Goose River Delta was measured on a composite aerial image taken from a helicopter in August 2012 during low flow and low tide. The distributary channels were counted where they met the shoreline and directly connected to flow coming from the trunk stream. The shoreline rugosity, morphology, and bathymetry of the Goose River Delta was mapped using single-beam and a RESON 7125SV2 200/400 kHz multibeam echo sounder (MBES) that was mounted off the port side of the R/V Lazarus research vessel. Dynamic positioning was provided by a Leica System 1230 real-time kinematic GPS, which provided relative horizontal positional accuracy to within 0.02 m. The MBES was linked to an Applanix POS-MV motion reference unit that provided real-time correction for boat movement. The MBES formed 512 beams over a 140 degree swath, with the swath width

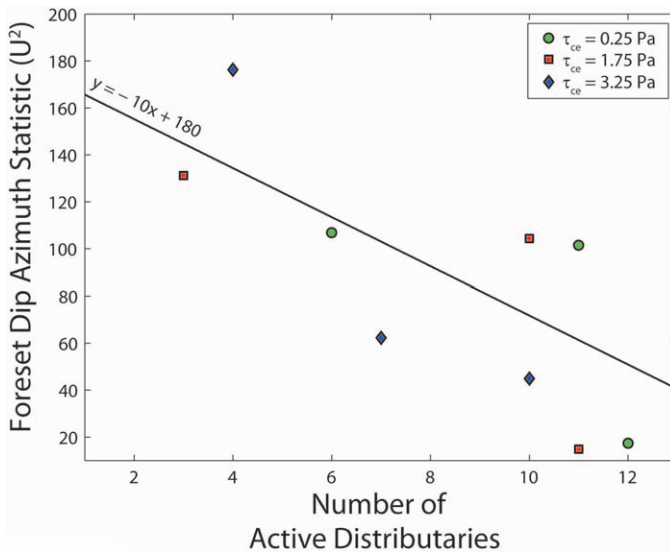


FIG. 4.—Foreset dip azimuth deviates less from a uniform circular distribution as the number of simultaneously active delta distributaries increases. With continued progradation these directionally variable foresets become clinoforms.

covering about five times the flow depth, and the measured vertical bed elevation was accurate to about 0.05 m. The MBES data were processed using CARIS HIPS to provide a digital elevation model at a 0.50 m grid spacing. We used the -1 m contour to define the shoreline because it is the shallowest reliable depth from the echosounder. This -1 m contour was not subject to the open-angle method because, unlike the modeled deltas, the contour did not enter any distributaries. The topset roughness was calculated from GPS elevation measurements along three partial strike lines. Clinoform dip magnitudes and concavities were obtained by importing multibeam data of the delta foreset into ArcGIS, calculating the slope at over two million points, and averaging. The proportion of channel and foreset facies could not be quantified due to the lack of channel facies represented in the few cut-bank outcrops.

The sub-bottom stratigraphy was imaged using an Innomar Parametric Echo Sounder (PES; see details in Wunderlich and Muller 2003; Lowag et al. 2012; Sambrook Smith et al. 2013) operating at two frequencies of 6 and 100 kHz. The PES was mounted from the port side of the R/V Lazarus, with its location also derived from the RTK dGPS, and the vessel heave corrected using an ORE motion reference unit mounted directly above the PES transducer on the PES pole. PES is especially effective in finer-grained sediments, but penetration is much reduced in sands. Although the PES achieved tens of meters of penetration in the glaciolacustrine sediments of Goose Bay, penetration on the sandy delta front was often only several meters.

Results

The southern active lobe of the Goose River Delta (Fig. 7C) is being constructed by roughly 14 active distributaries that contain at least five orders of bifurcation. The rugosity of the Goose River Delta shoreline is 2.1 and the topset roughness is 0.11 m. The average clinoform dip magnitude of the modern Goose River Delta foreset is 4° , with a standard deviation of 4.4° . The average clinoform concavity of the Goose River Delta is 9×10^{-5} , with a standard deviation of 2.8×10^{-5} . Sub-bottom profiles from one parametric echo line running offshore approximately normal to the delta front on the southern active lobe of the delta (Fig. 8) reveal several strong reflectors beneath the surface at a depth of 3–4 m, showing clinoform dips of c. 10 – 12° on the upper slope that decrease to c. 3° at the base. It is noticeable that the strength of the reflectors increases

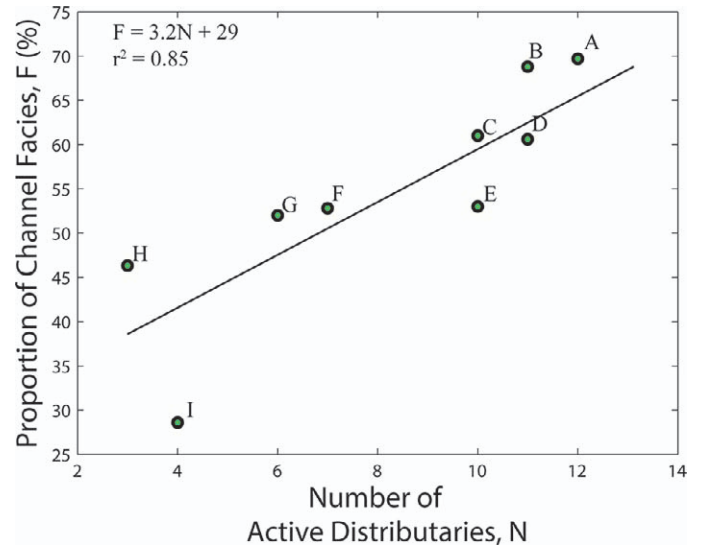


FIG. 5.—As the number of active distributaries increases, the proportion of channel facies also increases. The two variables are correlated with a coefficient of determination, $r^2 = 0.85$.

towards the base of the slope, as does the acoustic penetration, which probably reflects the finer grain sizes present at the base of the slope. At a depth of 16 m, the contemporary clinoform surface possess some undulations 1–1.5 m high, which are interpreted to be small slumps that have moved down the delta slope.

Discussion

Many of the topset attributes of the Goose River Delta are consistent with the predictions of the numerical model. For example, the distributaries of the Goose River Delta are consistent with the 12 distributaries and five orders of bifurcation predicted by Delft3D for a low cohesion, sand-dominated delta (Fig. 3A). The shoreline rugosity of 2.1 is consistent with, but lower than, the Delft3D prediction of 3.45 for a sandy, noncohesive delta (Fig. 3B). The observed topset roughness of 0.11 m is identical to the value predicted for a low-cohesion, sandy delta (Fig. 3C). Topsets in the numerical models become increasingly rough with decreasing sand and/or increasing cohesion, and as argued previously, this is a function of stabilization and aggradation of levees by cohesive fine-grained sediments. The Goose River Delta is sand-dominated and unvegetated, and as a result its levees do not aggrade.

Direct comparison of the clinoform dips for the Goose River and numerical deltas is not appropriate because the numerical deltas were modeled to prograde into much shallower water than the Goose River Delta. However, the steep clinoform dips of the modern Goose River Delta foreset plot closer in magnitude to the sand-dominated model deltas than the mud-dominated deltas. For comparison, the clinoform dip magnitudes of the fine-grained Atchafalaya Delta are less than 1° (Neill and Allison 2005) whereas clinoform dips of a coarse-grained Pennsylvanian delta in New Mexico (Gani and Bhattacharya 2005) are approximately 13° . Clinoform concavity is more readily compared with output from the numerical models because it is not as dependent on basin water depth. The average clinoform concavity of the Goose River Delta is most similar to the concavities of the sand-dominated numerical deltas (Fig. 3F), as is the clinoform dip azimuth statistic U^2 (Fig. 3E). In summary, we conclude that these observations of the morphology and clinoform geometry of the Goose River Delta are consistent with the model predictions for a low-cohesion, sand-dominated delta.

Regions of Net Sand Thicker than 0.5 m

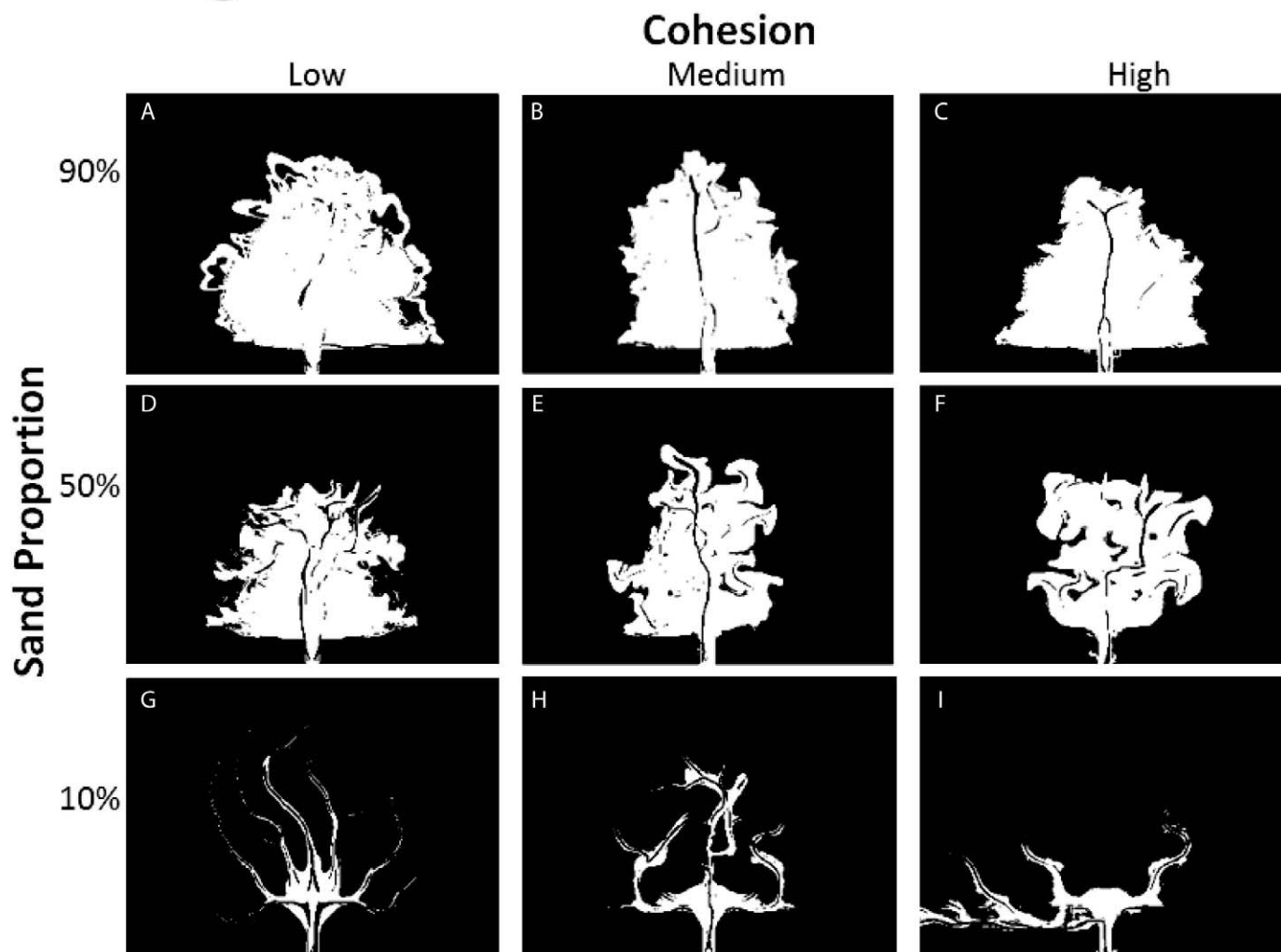


FIG. 6.—White areas outline regions where computed net sand thickness is greater than 0.5 m. Sand-body shapes vary from large and continuous for sand-dominated deltas to elongate and discontinuous for mud-dominated deltas.

APPLICATION OF MODEL PREDICTIONS

A common objective of paleoenvironmental interpretation is to infer the three-dimensional sedimentary architecture of deposits from limited data such as 2D seismic or outcrop cross sections. In hydrocarbon exploration, this exercise is typically undertaken in order to generate a reservoir model and mitigate reservoir uncertainties arising from limited data. Our approach towards this end is to quantify the clinoform dip magnitude, clinoform concavity, and facies distributions from outcrop cross sections and use these measurements, combined with the Delft3D predictions, to hindcast the planform shoreline rugosity, topset roughness, and number of active distributaries of the paleodelta. These parameters in turn provide a more quantitative prediction of ancient delta planform that can be used to infer the three-dimensional architecture of a paleodelta. The example we use herein to test this application is the Cretaceous Last Chance Delta of the Ferron Sandstone, near Emery, Utah, USA (Fig. 9).

Geologic Setting

The Upper Ferron Sandstone Member of the Cretaceous (Turonian) Mancos Shale Formation was deposited by the Last Chance Delta (90.3–88.6 Ma), one of the most studied of all ancient deltas exposed in outcrop (Katich 1953, Hale and Van De Graaff 1964; Cotter 1975; Ryer 1981; Gardner 1992; Lowry and Jacobsen 1993; Gardner et al. 1995; Gardner 1995; Barton 1997; Garrison et al. 1997; Corbeau et al. 2001; Novakovic et al. 2002; Bhattacharya and Tye 2004; Moiola et al. 2004; Ryer and Anderson 2004; Enge et al. 2010). Seven fluvial–deltaic parasequence sets (Kf-1 through Kf-7) are exposed in the vertical cliffs of Castle Valley near the western flank of the San Rafael Swell (Fig. 9). They were deposited as part of the Southern Utah Deltaic Complex of the Cretaceous Western Interior Seaway (Garrison and van den Bergh 2004). Here we restrict our discussion to the Kf-1 parasequence set.

Several studies have reconstructed the paleomorphology and paleoenvironment of the Last Chance Delta. Hale and Van De Graaff (1964)

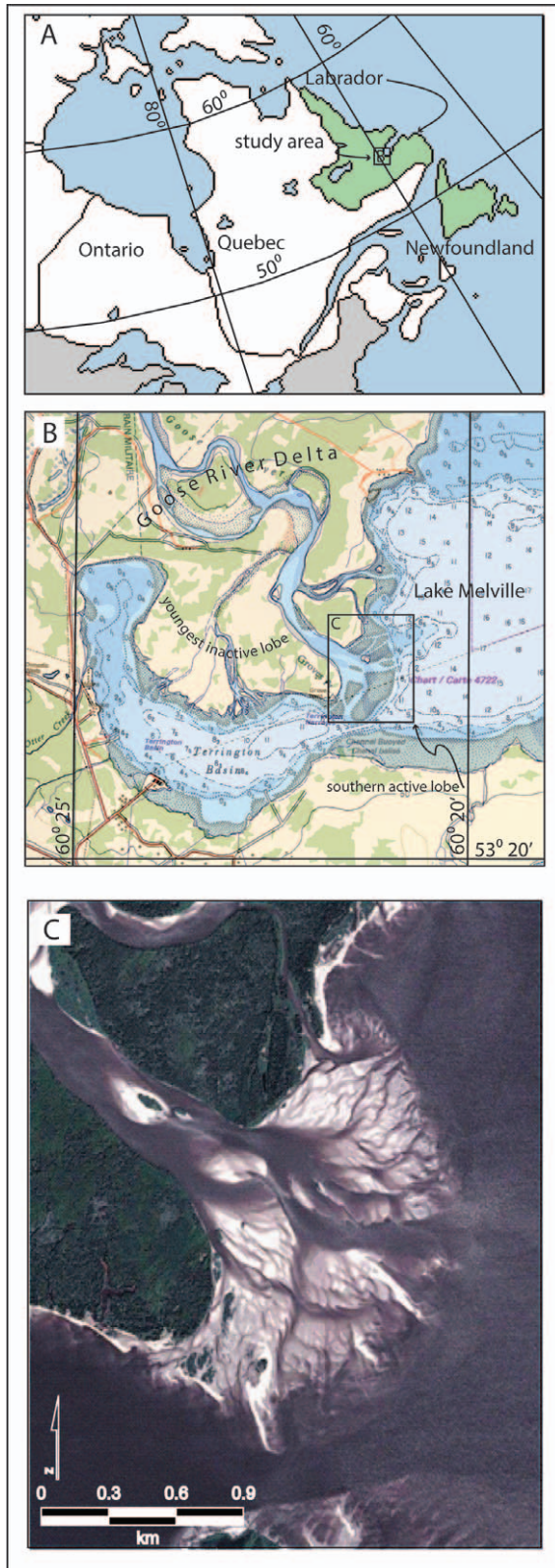


FIG. 7.—A) Goose River Delta is located in Labrador, Canada at the western end of B) Lake Melville, a fjord weakly connected to the Labrador Sea to the east. Youngest inactive lobe as labeled; of the two active, sandy, unvegetated lobes, the southern one is indicated by the box in Part B. C) Aerial photograph of area on box in Part B (image B modified from ESRI World Topographic Basemap).

were the first to propose a paleogeographic reconstruction as a lobate delta. Cotter (1976) described the paleoshoreline as “a broad fan, smaller parts of which were sub-delta lobes” (Fig. 10A) and estimated that the delta prograded into a water depth of c. 12 m. Thompson et al. (1986) envisioned a river-dominated lobate delta whose shoreline was remolded into barrier islands (Fig. 10B). Gardner (1992) (Fig. 10C) and Edwards et al. (2005) quoting Gardner et al. (1995) (Fig. 10D), realized that parasequence sets Kf-1 through Kf-3 were deposited in a more river-dominated delta system than the higher more wave-influenced parasequences. Gardner et al. (1992) for example, in their figure 53 specifically depict Kf-1 and Kf-2 as a river-dominated, birdsfoot delta with “pronounced elongate to lobate coastline morphologies” (quoted from the figure caption). Anderson and Ryer (2004) favor a composite character (Fig. 10E), showing the Last Chance Delta with a fan-like eastern component and a rugose birdsfoot northwestern component. Many studies have attributed the river-dominated morphology of the delta to progradation roughly due north into an embayment that provided protection from waves and storms and may have had a reduced salinity (Cotter 1976; Bhattacharya and Davies 2001; Anderson and Ryer 2004). Bhattacharya and Tye (2004) suggested that the Last Chance Delta “experienced only a few orders of bifurcation” and that its shoreline was “wave-influenced.” Anderson and Ryer (2004) also argued that there may have been as few as two orders of bifurcation in the Last Chance Delta and that the two lowermost parasequence sets (Kf-1 and Kf-2) were likely “formed within embayments” as a component of an “asymmetric wave-influenced delta.” The Mississippi Delta has been proposed as a modern analog to the Last Chance Delta (Cotter 1975; Muiola et al. 2004), although Bhattacharya and Tye (2004) view the Brazos, Ebro, and Rhone deltas as better analogs.

In summary, despite excellent cross sectional exposures, there are conflicting views on the paleomorphology of the Last Chance Delta. Some of the conflict may arise because earlier authors presented conceptual qualitative models that in some cases amalgamate two million years of deposition, but there are various interpretations even for the Kf-1 and Kf-2 parasequence sets. Our data come from Kf-1, and our model runs are more appropriately compared to these river-dominated progradational parasequence sets, whose duration of deposition according to Gardner et al. (2004) is approx. 300,000 yr. Here we use the stratigraphic variables defined earlier to compare the clinof orm geometry of the Last Chance Kf-1 delta with Delft3D predictions with the goal of hindcasting its topset attributes.

Methods

A comparison of the Last Chance Delta to our model predictions requires us to place the Kf-1 Last Chance Delta within our model parameter space. The trunk stream of the Last Chance Delta is estimated to have drained an area of 50,000 km² of the Sevier orogenic highlands which produced an estimated maximum discharge of 1,250 m³ s⁻¹ (Bhattacharya and Tye 2004), comparable with the 1,000 m³ s⁻¹ used to construct our modeled deltas. The tidal range at the river mouth was likely microtidal (Ryer and Anderson 2004), and the wave climate during deposition of Kf-1 was not sufficient to produce appreciable hummocky cross-stratified beds. The progradation distance of Kf-1 also suggests that the wave climate was not strong enough to induce longshore transport capable of impeding progradation. Bhattacharya and MacEachern (2009) suggest that the Ferron rivers depositing Kf-1 were frequently hyperpycnal, allowing the suspended load to bypass the delta front. We do not include hyperpycnal flows in the model simulations. As noted above, flume experiments by Kostic and Parker (2003a, 2003b) demonstrate that muddy turbidity currents on a sandy foreset will reduce the foreset angle by 20%, although the process of angle reduction is self-limiting.

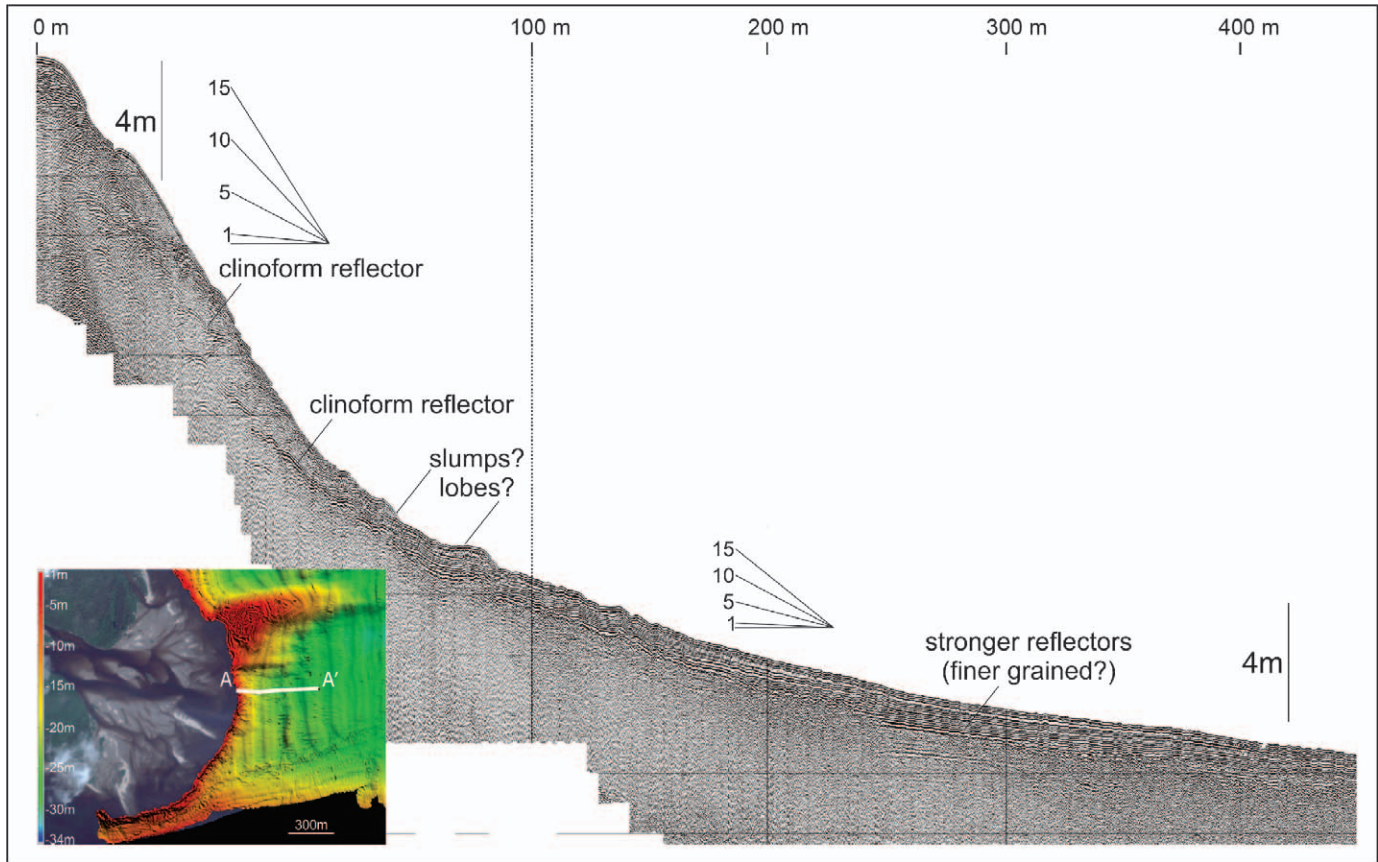


Fig. 8.—Parametric echo sounder (PES) sub-bottom profiles from a survey line running offshore approximately normal to the delta front on the southern active lobe of the delta (inset MBES map shows location). Note horizontal scale change at distances less than 100 m, and the two different slope-angle indicators for these locations. The contemporary clinoform surface is steepest (c. 12°) on the upper delta slope and decreases to c. 3° at the slope base. Small slumps are present at around 16 m water depth, with the strength of the reflectors and depth of acoustic penetration being greater near the base of slope, reflecting the finer grain sizes there.

The extent to which hyperpycnal flows will change the other parameters is unknown.

The proportions of sand and mud transported by the trunk stream of the Last Chance Delta also are unknown; Bhattacharya and Tye (2004) argue that the Ferron river system was similar to a modern, moderate-size, sandy bedload river and that modern large, mud-dominated rivers

are not an appropriate analog. But as argued above, to place the Kf-1 Last Chance Delta in the morphology space of Figure 1, it is more important to know the proportions of noncohesive and cohesive fractions in the delta itself. The estimated proportion of sand deposited in the Last Chance Delta was determined by calculating the relative proportions of sand (greater than lower very fine) and mud (less than lower very fine) in



Fig. 9.—A) Outcrop belt of the Ferron Sandstone (black) in the Emery, Utah area (modified from Zeng et al. 2004); locations of areas mentioned in text indicated by rectangles. B) Leftward-dipping clinoforms of the Last Chance Delta (parasequence set Kf-1-Iv[a] of Anderson et al. 2003) on the north side of I-70 along Ivie Creek. Bar indicates 12 m.

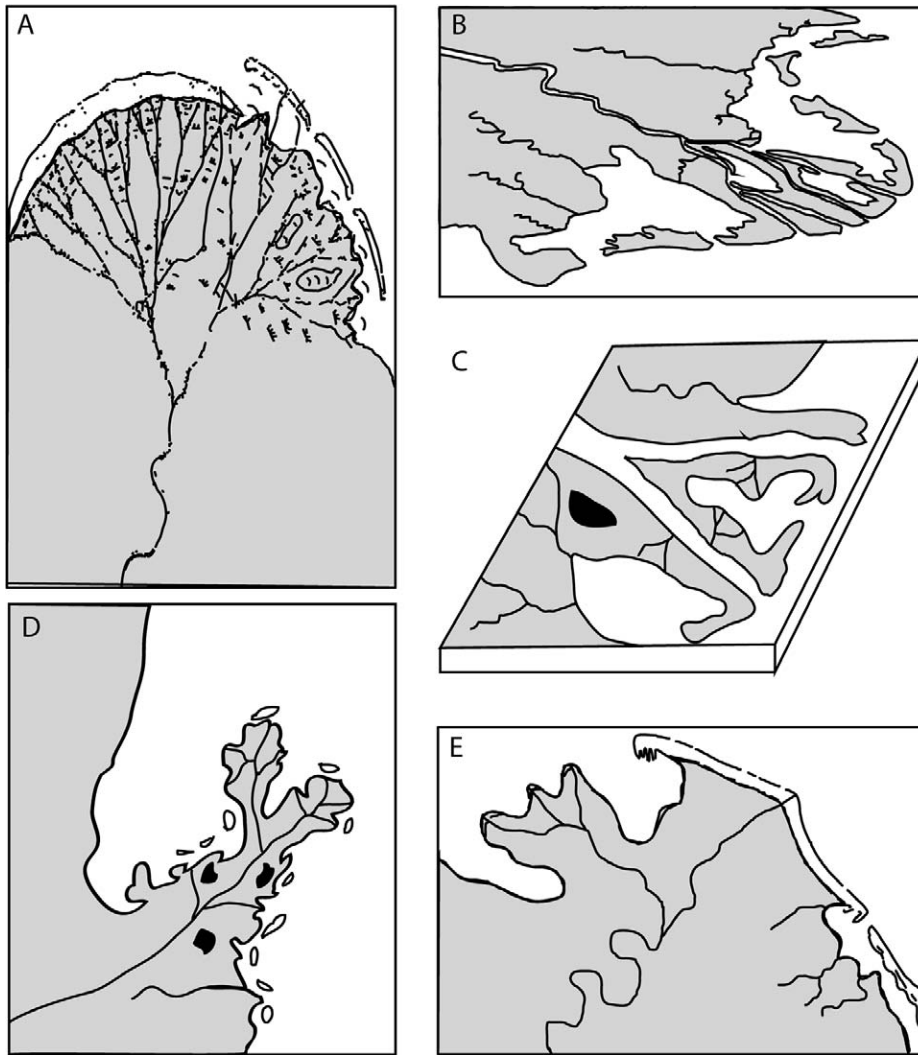


FIG. 10.—Paleogeographies of the Last Chance Delta induced from cores and outcrop by various authors (not to scale and un-oriented with respect to north). **A)** Cotter (1976) interpreted the Last Chance Delta as a broad, fan-shaped complex formed by coalescing lobes having numerous distributaries and bifurcations. **B)** Thompson et al. (1986) generally concurred with Cotter, envisioning a river-dominated, lobate delta fed by several distributaries whose shorelines were reworked into barrier islands fronting back bays. **C)** Gardner (1992) and **D)** Edwards et al. (2005) quoting Gardner et al. (1995), realized that parasequence sets Kf-1 through Kf-3 were deposited in a more river-dominated delta system than the higher more wave-influenced parasequences, under conditions of relative base-level fall. They interpreted the paleogeography at this time as a fluvially dominated elongate delta complex with a lobate shoreline. **E)** Anderson and Ryer (2004) reflect this composite character, showing the Last Chance Delta with a fan-like eastern component and a rugose birdsfoot northwestern component.

vertical sections measured by the Utah State Geological Survey (Anderson et al. 2003). The proportion of sand was quantified by comparing the vertical thicknesses of sand deposits in Kf-1 with the total preserved thickness of Kf-1 in six measured sections in the Rock Canyon and Ivie Creek areas (Fig. 9). The average sand proportion of Kf-1 by this calculation is 81%. According to Mattson and Chan (2004), the D_{50} of the sand in the Kf-1-Iv[a] parasequence lies between the very fine and fine size classes. This falls between the D_{50} of 177 μm and 80 μm used in the sand-dominated and sand-mixed model runs. The Last Chance Delta formed in a humid, tropical to subtropical environment at paleolatitudes of 45–55° N (Bhattacharya and MacEachern 2009), and its coal deposits are in excess of 1 m thick. These conditions are indicative of a highly vegetated topset that may have increased its effective sediment cohesion, but we do not yet know how to quantify this effect.

The water depth into which the Last Chance Delta prograded has been estimated from clinoform thicknesses. In the Ivie Creek area, the sandy clinoforms of Kf-1 are 6–12 m thick and pinch out rapidly down-dip into subhorizontal, lenticular-bedded mudstones containing thin, wave-rippled cross-laminated sandstones. This implies that the sea floor was above storm wave base, and water depths were greater than 10 m, but probably not more than 30 m. This is 3 to 10 times the basin depth of 3.5 m in the model runs. The influence of initial basin depth on the variables measured in this study is presently unknown but is a subject of future study.

The evolution of base level during deposition of the Kf-1 and Kf-2 is controversial. Gardner (1995) thought that Kf-1 through Kf-3 were deposited under conditions of relative base-level fall, whereas Enge and Howell (2010) saw a climbing trajectory for coastal-plain deposits of Kf-1-Ivie Creek[a], interpreted as indicating a steadily rising sea level. In the face of these contradictions, an assumption of steady base level seems appropriate.

Of the seven variables identified in Equation 1, four are measurable in exposures of the Last Chance Delta: i) channel facies proportion, ii) clinoform dip magnitude, iii) clinoform dip azimuth statistic, and iv) clinoform concavity. The proportions of channel and foreset facies were calculated from photomosaics given in Utah Geological Survey Open File Report 412 (Anderson et al. 2003). Fifty photomosaics were selected by a random-number generator from a list of roughly 150 photomosaics where Kf-1 is exposed in outcrop, thereby filtering out any bias due to the relative proximal or distal position of any particular group of photos. Facies measurements were made on these photos for all parasequences within the first parasequence set (Kf-1). Channel facies were mapped where Anderson et al. (2003) identified channel bodies or distributaries belonging to Kf-1. Foreset facies were mapped where Anderson et al. (2003) identified sand bodies that were either “wave-dominated nearshore marine,” “wave-modified nearshore marine,” or “fluvial-dominated nearshore marine.” The true dips and concavities of the clinoforms were measured from multiple parasequences in the Kf-1 parasequence set, and

the clinof orm dip azimuth statistic was computed from true clinof orm dip azimuth data calculated from 3D outcrop exposures. For each photomosaic, we collected a GPS position at a location in the field from which a laser rangefinder was used to obtain horizontal and vertical distances, and azimuths of prominent bedding surfaces. The clinof orm surfaces were measured where they were identifiable on both the outcrop and the photomosaic. Where this was not possible, the laser rangefinder data were gathered at evenly spaced intervals along the photomosaic, which permitted clinof orm measurement after the photomosaics were geo-referenced. Data were collected from thirty photomosaics, the images were geo-referenced, and then the point data on the photos were converted to spherical coordinates. From the geo-referenced photos, 88 apparent clinof orm dip magnitudes were computed using two points along a clinof orm surface exposed on a face, 33 clinof orm concavities were measured, and 46 true clinof orm dip azimuths were trigonometrically computed using time-equivalent apparent clinof orm dips on two adjacent cliff faces.

Results

The magnitudes of apparent clinof orm dip in the Last Chance Delta range from near zero degrees to a maximum of 15.5°, with an average of 4° and standard deviation of 4°. The clinof orm dip-azimuth statistic based on the 46 true dip azimuths is 1.1. Average clinof orm concavity is 1.3×10^{-4} . Eighty-eight percent of the Last Chance Delta deposits are foreset facies, although this number probably is biased by the ravinement unconformity at the top of the parasequence set; 12% of the deposit is channel facies.

Determining the Paleomorphology of the Last Chance Delta

Comparison of clinof orm dip magnitudes, azimuth variation, and concavity from the Kf-1 Last Chance Delta with the relevant plots in Figure 3 indicates that the Kf-1 Last Chance Delta was most similar to model deltas Figure 1B and 1E, intermediate between a fan and a birdsfoot delta. Its proportion of channel facies is less than predicted, but we attribute this to topset ravinement during transgression and relatively immobile channels (due to heavily vegetated banks) that minimized the creation of channelized facies. The delta probably was constructed by numerous distributaries with at least five orders of bifurcation. The two orders of bifurcations, recognized by Bhattacharya and Tye (2004) and Anderson and Ryer (2004), likely represent only lower-order, deeper channels that escaped erosion during the subsequent transgression.

CONCLUSIONS

Our objective has been to better quantify the functional relationships between the sediment type of a delta and its morphology and stratigraphy. Based on numerical modeling using Delft3D and observations from the coarse-grained Goose River Delta, we conclude that in the absence of appreciable waves and tides, a relatively noncohesive, sandy delta will have more active distributaries, a less rugose shoreline morphology, less topset relief, and less variability in foreset dip directions than a highly cohesive, muddy delta. Thus, variations in the caliber of sediment delivered to, and retained in, a delta play a more important role than previously appreciated in setting the distributary abundance, shoreline rugosity, topset roughness, and foreset dip variability of river-dominated deltas. These, in turn, control sediment deposition and impact the stratigraphy of the delta by controlling clinof orm dip magnitudes, clinof orm concavities, the proportion of channel and foreset facies, and sand-body geometries.

Application of these results to the Cretaceous Last Chance Delta of the Ferron Sandstone in central Utah indicates how the preserved

stratigraphic attributes, such as clinof orm dip magnitude, dip-azimuth variability, and concavity, can be inverted to predict the planform of an ancient delta. The Last Chance Delta was most likely a modified fan delta having a quasi-regular shoreline fed by numerous distributaries that crossed a relatively low-relief delta top.

SUPPLEMENTAL MATERIAL

Run 1 is available from JSR's Data Archive: <http://sepm.org/pages.aspx?pageid=229>.

ACKNOWLEDGMENTS

Our thanks to Michael Arthur and Elizabeth Hajek for reading earlier versions of the manuscript and to Sarah Prozeller for assistance in the field. The manuscript greatly benefited from comments by two anonymous reviewers. This research has been funded by National Science Foundation grants OCE-061495 and FESD/EAR-1135427 awarded to R.L. Slingerland, grants OCE 1061380 and FESD/EAR-1135427 awarded to D.A. Edmonds, grant NE/E001661/1 awarded to D. Parsons, and grant EAR-0809653 awarded to R.L. Slingerland and J. Best.

REFERENCES

- ANONYMOUS, 2001, Aquatic environment in the Goose Bay estuary: Technical Report TF1 0404 on the Labrador Hydro Project, 1998–1999 Environmental Studies, Volume 1, AMEC Earth and Environmental Limited, 95 Bonaventure Avenue, P.O. Box 2035, St. John's, NF A1C 5R6 and BAE-NewPlan Group Limited, SNC-Lavalin, 1133 Topsail Road, Mount Pearl, NF A1N 2W4, Canada.
- ANDERSON, P., AND RYER, T., 2004, "Regional stratigraphy of the Ferron Sandstone." Regional to wellbore analog for fluvial-deltaic reservoir modeling: The Ferron Sandstone of Utah: American Association of Petroleum Geologists, Studies in Geology, v. 50, p. 211–224.
- ANDERSON, P., MCCLURE, K., CHIDSEY, T., JR., RYER, T., MORRIS, T., DEWEY, J., JR., AND ADAMS, R., 2003, Interpreted regional photomosaics and cross section, Cretaceous Ferron Sandstone, east-central Utah: Utah Geological Survey, Open-File Report 412.
- BARTON, M.D., 1997, Application of Cretaceous Interior seaway outcrop investigations to fluvial-deltaic reservoir characterization: Part 1. Predicting reservoir heterogeneity in delta front sandstones, Ferron gas field, central Utah, in Shanley, K.W., and Perkins, R.F., eds., *Shallow Marine and Nonmarine Reservoirs, Sequence Stratigraphy, Reservoir Architecture and Production Characteristics*: SEPM, Gulf Coast Section, 18th Annual Research Conference, p. 33–40.
- BHATTACHARYA, J.P., 2006, Deltas, in Posamentier, H.W., and Walker, R.G., eds., *Facies Models Revisited*: SEPM, Special Publication 84, p. 237–292.
- BHATTACHARYA, J.P., AND DAVIES, R.K., 2001, Growth faults at the prodelta to delta-front transition, Cretaceous Ferron sandstone, Utah: *Marine and Petroleum Geology*, v. 18, p. 525–534.
- BHATTACHARYA, J., AND MAC EACHERN, J., 2009, Hyperpycnal rivers and prodeltaic shelves in the Cretaceous seaway of North America: *Journal of Sedimentary Research*, v. 79, p. 184–209.
- BHATTACHARYA, J.P., AND TYE, R.S., 2004, Searching for modern Ferron analogs and application to subsurface interpretation, in Chidsey, T., Jr., Adams, R., and Morris, T., eds., *Analog for Fluvial-Deltaic Reservoir Modeling: Ferron Sandstone of Utah*: American Association of Petroleum Geologists, Studies in Geology, v. 50, p. 39–58.
- CALDWELL, R.L., AND EDMONDS, D.A., 2014, The effects of sediment properties on deltaic processes and morphologies: a numerical modeling study: *Journal of Geophysical Research: Earth Surface*, v. 119, p. 2013JF002965.
- CARLSON, B., KIM, W., AND PILIOURAS, A., 2013, Basin Depth Control on the Autogenic Timescale of Fluviodeltaic Systems [Abstract]: American Geophysical Union, Fall Meeting Abstracts, v. 1, p. 4.
- CEDERBERG, J., 2014, A quantitative assessment of the effects of base level fall and basin depth on river-dominated deltas [MA thesis]: The Pennsylvania State University, <http://cat.libraries.psu.edu/uhtbin/cgiirsi/?ps=HPQikfkm5t/UP-PAT/229700367/9>.
- COACHMAN, L.K., 1953, River flow and winter hydrograph structure of the Hamilton Inlet-Lake Melville estuary of Labrador: Blue Dolphin Labrador Expedition, Winter Project, unpublished manuscript, 19 p., available at: <http://www.dtic.mil/dtic/tr/fulltext/u2/021124.pdf>.
- CLARK, P.U., AND FITZHUGH, W.W., 1992, Postglacial relative sea level history of the Labrador coast and interpretation of the archaeological record, in Johnson, L.L., and Stright, M., eds., *Paleoshorelines and Prehistory: An Investigation of Method*: Boca Raton, CRC Press, 189 p.
- COLEMAN, J.M., AND PRIOR, D.B., 1982, Deltaic environments, in Scholle, P.A., and Spearing, D.R., eds., *Sandstone Depositional Environments*: American Association of Petroleum Geologists, Memoir 31, p. 139–178.

- CORBEANU, R.M., SOEGAARD, K., SZERBIAK, R.B., THURMOND, J.B., MCMEECHAN, G.A., WANG, D., SNELGROVE, S., FORSTER, C.B., AND MENITOVE, A., 2001, Detailed internal architecture of a fluvial channel sandstone determined from outcrop, cores, and 3-D ground-penetrating radar: Example from the middle Cretaceous Ferron Sandstone, east-central Utah: *American Association of Petroleum Geologists, Bulletin*, v. 85, p. 1583–1608.
- COTTER, E., 1975, Deltaic deposits in the Upper Cretaceous Ferron Sandstone, Utah, in Broussard, M.L., ed., *Deltas: Models for Exploration*: Houston, Texas, Houston Geological Society, p. 471–483.
- COTTER, E., 1976, The role of deltas in the evolution of the Ferron Sandstone and its coal, Castle Valley, Utah: Brigham Young University, *Geology Studies*, v. 22, p. 15–41.
- DRISCOLL, N.W., AND KARNER, G.D., 1999, Three-dimensional quantitative modeling of clinoform development: *Marine Geology*, v. 154, p. 383–398.
- EDMONDS, D.A., AND SLINGERLAND, R.L., 2007, Mechanics of river mouth bar formation: implications for the morphodynamics of delta distributary networks: *Journal of Geophysical Research*, v. 112, F02034.
- EDMONDS, D.A., AND SLINGERLAND, R.L., 2008, Stability of delta distributary networks and their bifurcations: *Water Resources Research*, v. 44, W09426.
- EDMONDS, D.A., AND SLINGERLAND, R.L., 2010, Significant effect of sediment cohesion on delta morphology: *Nature Geoscience*, v. 3, p. 105–109.
- EDMONDS, D.A., PAOLA, C., HOYAL, D.C.J.D., AND SHEETS, B.A., 2011a, Quantitative metrics that describe river deltas and their channel networks: *Journal of Geophysical Research*, v. 116, F04022.
- EDMONDS, D.A., SHAW, J.B., AND MOHRIG, D., 2011b, Topset-dominated deltas: a new model for river delta stratigraphy: *Geology*, v. 39, p. 1175–1178.
- EDWARDS, C.M., HOWELL, J.A., AND FLINT, S.S., 2005, Depositional and stratigraphic architecture of the Santonian Emery Sandstone of the Mancos Shale: implications for Late Cretaceous evolution of the Western Interior Foreland Basin of central Utah, *USA: Journal of Sedimentary Research*, v. 75, p. 280–299.
- ENGE, A.D., AND HOWELL, J.A., 2010, Impact of deltaic clinothems on reservoir performance: Dynamic studies of reservoir analogs from the Ferron Sandstone Member and Panther Tongue, Utah: *American Association of Petroleum Geologists, Bulletin*, v. 94, p. 139–161.
- ENGE, A.D., HOWELL, J.A., AND BUCKLEY, S.J., 2010, The geometry and internal architecture of stream mouth bars in the Panther Tongue and Ferron Sandstone Members, Utah, U.S.A.: *Journal of Sedimentary Research*, v. 80, p. 1018–1031.
- FALCINI, F., AND JEROLMACK, D.J., 2010, A potential vorticity theory for the formation of elongate channels in river deltas and lakes: *Journal of Geophysical Research Earth Surface*, v. 115, no. F04038.
- FIELDING, C.R., TRUEMAN, J., AND ALEXANDER, J., 2005, Sedimentology of the Modern and Holocene Burdekin River Delta of North Queensland, Australia: controlled by river output, not by waves and tides, in Giosan, L., and Bhattacharya, J.P., eds., *River Deltas: Concepts, Models, and Examples*: SEPM, Special Publication, v. 83, p. 467–496.
- GALLOWAY, W.E., 1975, Process framework for describing the morphologic and stratigraphic evolution of deltaic depositional systems, in Broussard, M.L., ed., *Deltas: Models for Exploration*: Houston, Texas, Houston Geological Society, p. 87–98.
- GANI, M.R., AND BHATTACHARYA, J.P., 2005, Lithostratigraphy versus chronostratigraphy in facies correlations of Quaternary deltas: application of bedding correlation, in Giosan, L., and Bhattacharya, J.P., eds., *River Deltas: Concepts, Models, and Examples*: SEPM, Special Publication, v. 83, p. 31–48.
- GARDNER, M.H., 1992, Sequence stratigraphy of the Ferron Sandstone (Turonian) of East-Central Utah [unpublished Ph. D. dissertation]: Colorado School of Mines, Golden, Colorado, 406 p.
- GARDNER, M.H., 1995, The stratigraphic hierarchy and tectonic history of the mid-Cretaceous foreland basin of central Utah, in Dorobek, S.L., and Ross, G.M., eds., *Stratigraphic Evolution of Foreland Basins*: SEPM, Special Publication 52, p. 283–303.
- GARDNER, M., WILLIS, B., AND BARTON, M., 1995, Accommodation controls on fluvial-deltaic reservoir architecture: *American Association of Petroleum Geologists, Search and Discovery Article #90956*, International Convention and Exposition Meeting, Nice, France.
- GARDNER, M.H., CROSS, T.A., AND LEVORSEN, M., 2004, Stacking patterns, sediment volume partitioning, and facies differentiation in shallow-marine and coastal-plain strata of the Cretaceous Ferron Sandstone, Utah, in Chidsey, T.C., Jr., Adams, R.D., and Morris, T.H., eds., *Regional to Wellbore Analog for Fluvial-Deltaic Reservoir Modeling: the Ferron Sandstone of Utah*: American Association of Petroleum Geologists, *Studies in Geology* 50, p. 95–124.
- GARRISON, J.R., AND VAN DEN BERGH, T.C., 2004, The high-resolution depositional sequence stratigraphy of the Upper Ferron Sandstone, Last Chance Delta: an application of coal zone stratigraphy, in Chidsey, T.C., Jr., Adams, R.D., and Morris, T.H., eds., *Regional to Wellbore Analog for Fluvial-Deltaic Reservoir Modeling: the Ferron Sandstone of Utah*: American Association of Petroleum Geologists, *Studies in Geology* 50, p. 125–192.
- GARRISON, J., VAN DEN BERGH, T., BARKER, C.E., AND TABET, D.E., 1997, Depositional sequence stratigraphy and architecture of the Cretaceous Ferron Sandstone: implications for coal and coalbed methane resources: a field excursion: Brigham Young University, *Geology Studies*, v. 42, p. 155–202.
- GELEYNSE, N., STORMS, J.E.A., WALSTRA, D.J.R., JAGERS, H., WANG, Z.B., AND STIVE, M.J.F., 2011, Controls on river delta formation: insights from numerical modelling: *Earth and Planetary Science Letters*, v. 302, p. 217–226.
- GIOSAN, L., DONNELLY, J., VESPREMEANU, E., BHATTACHARYA, J.P., OLARIU, C., AND BUONAIUTO, F., 2005, River delta morphodynamics: examples from the Danube delta, in Giosan, L., and Bhattacharya, J.P., eds., *River Deltas: Concepts, Models, and Examples*: SEPM, Special Publication 83, p. 87–132.
- HALE, L.A., AND VAN DE GRAAFF, F.R., 1964, Cretaceous stratigraphy and facies patterns: northeastern Utah and adjacent areas: Intermountain Association of Petroleum Geologists, 13th Annual Field Conference, Guidebook to the Geology and Mineral Resources of the Uinta Basin, Utah's Hydrocarbon Storehouse, p. 115–138.
- JONES, T.A., 2006, MATLAB functions to analyze directional (azimuthal) data, I: single-sample inference: *Computers & Geosciences*, v. 32, p. 166–175.
- JOPLING, A.V., 1966, Some applications of theory and experiment to the study of bedding genesis: *Sedimentology*, v. 7, p. 71–102.
- KATICH, P.J., JR., 1953, Source direction of Ferron Sandstone in Utah: *American Association of Petroleum Geologists, Bulletin*, v. 37, p. 858–861.
- KOSTIC, S., AND PARKER, G., 2003a, Progradational sand-mud deltas in lakes and reservoirs; Part 1, Theory and numerical modeling: *Journal of Hydraulic Research*, v. 41, p. 127–140.
- KOSTIC, S., AND PARKER, G., 2003b, Progradational sand-mud deltas in lakes and reservoirs, Part 2, experimental and numerical simulation: *Journal of Hydraulic Research*, v. 41, p. 141–152.
- KUEHL, S.A., NITTROUER, C.A., AND DEMASTER, D.J., 1986, Distribution of sedimentary structures in the Amazon subaqueous delta: *Continental Shelf Research*, v. 6, p. 311–336.
- LAMBIASE, J.J., DAMIT, A.R., SIMMONS, M.D., ABDOERRIAS, R., AND HUSSIN, A., 2003, A depositional model and the stratigraphic development of modern and ancient tide-dominated deltas in NW Borneo, in Sidi, F.H., Nummedal, D., Imbert, P., Darman, H., and Posamentier, H.W., eds., *Tropical Deltas of Southeast Asia: Sedimentology, Stratigraphy, and Petroleum Geology*: SEPM, Special Publication 76, p. 109–123.
- LESSER, G., ROELVINK, J., VAN KESTER, J., AND STELLING, G., 2004, Development and validation of a three-dimensional morphological model: *Coastal Engineering*, v. 51, p. 883–915.
- LIVERMAN, D.G.E., 1997, Quaternary Geology of the Goose Bay Area, Newfoundland: Newfoundland Department of Mines and Energy, Geological Survey, Report 97-1, p. 173–182.
- LOWAG, J., BULL, J.M., VARDY, M.E., MILLER, H., AND PINSON, L.J.W., 2012, High-resolution seismic imaging of a Younger Dryas and Holocene mass movement complex in glacial lake Windermere, UK: *Geomorphology*, v. 171–172, p. 42–57.
- LOWRY, P., AND JACOBSEN, T., 1993, Sedimentological and reservoir characteristics of a fluvial-dominated delta-front sequence: Ferron Sandstone Member (Turonian), east-central Utah, USA, in Ashton, M., ed., *Geological Society of London, Special Publication* 69, p. 81–103.
- MARCIANO, R., WANG, Z.B., HIBMA, A., DE VRIEND, H.J., AND DEFINA, A., 2005, Modeling of channel patterns in short tidal basins: *Journal of Geophysical Research*, v. 110, F01001.
- MATTSON, A., AND CHAN, M.A., 2004, Facies and permeability relationships for wave-modified and fluvial-dominated deposits of the Cretaceous Ferron Sandstone, central Utah, in Chidsey, T.C., Jr., Adams, R.D., and Morris, T.H., *Regional to Wellbore Analog for Fluvial-Deltaic Reservoir Modeling: the Ferron Sandstone of Utah*: American Association of Petroleum Geologists, *Studies in Geology* 50, p. 251–275.
- MCPHERSON, J.G., SHANMUGAM, G., AND MOIOLA, R.J., 1987, Fan-deltas and braid deltas: varieties of coarse-grained deltas: *Geological Society of America, Bulletin*, v. 99, p. 331–340.
- MITCHUM, R.M., JR., VAIL, P.R., AND SANGREE, J.B., 1977, Seismic stratigraphy and global changes of sea level, Part 6, stratigraphic interpretation of seismic reflection patterns in depositional sequences, in Payton, C.E., ed., *Seismic Stratigraphy: Applications to Hydrocarbon Exploration*: American Association of Petroleum Geologists, *Memoir* 26, p. 135–143.
- MOIOLA, R.J., WELTON, J. E., WAGNER, J.B., FEARN, L.B., FARRELL, M.E., AND ENRICO, R.J., 2004, Integrated analysis of the Upper Ferron deltaic complex, southern Castle Valley, Utah: Analog for fluvial-deltaic reservoir modeling, in Chidsey, T.C., Jr., Adams, R.D., and Morris, T.H., *Regional to Wellbore Analog for Fluvial-Deltaic Reservoir Modeling: the Ferron Sandstone of Utah*: American Association of Petroleum Geologists, *Studies in Geology* 50, p. 79–91.
- NEILL, C.F., AND ALLISON, M.A., 2005, Subaqueous deltaic formation on the Atchafalaya Shelf, Louisiana: *Marine Geology*, v. 214, p. 411–430.
- NIEDORODA, A.W., REED, C.W., DAS, H., FAGHERAZZI, S., DONOGHUE, J.F., AND CATTANEO, A., 2005, Analyses of a large-scale depositional clinoformal wedge along the Italian Adriatic coast: *Marine Geology*, v. 222, p. 179–192.
- NITTROUER, C.A., KUEHL, S.A., DEMASTER, D.J., AND KOWSMANN, R.O., 1986, The deltaic nature of Amazon shelf sedimentation: *Geological Society of America, Bulletin*, v. 97, p. 444–458.
- NITTROUER, C.A., KUEHL, S.A., STERNBERG, R.W., FIGUEIREDO, A.G., JR., AND FARIA, L.E.C., 1995, An introduction to the geological significance of sediment transport and accumulation on the Amazon continental shelf: *Marine Geology*, v. 125, p. 177–192.
- NOVAKOVIC, D., WHITE, C.D., CORBEANU, R.M., HAMMON, W.S., III, BHATTACHARYA, J.P., AND MCMEECHAN, G.A., 2002, Hydraulic Effects of shales in fluvial-deltaic deposits: ground-penetrating radar, outcrop observations, geostatistics, and three dimensional flow modeling for the Ferron Sandstone, Utah: *Mathematical Geology*, v. 34, p. 857–893.
- OLARIU, C., AND BHATTACHARYA, J.P., 2006, Terminal distributary channels and delta front architecture of river-dominated delta systems: *Journal of Sedimentary Research*, v. 76, p. 212–233.

- ORTON, G.J., AND READING, H.G., 1993, Variability of deltaic processes in terms of sediment supply, with particular emphasis on grain size: *Sedimentology*, v. 40, p. 475–512.
- PAOLA, C., MULLIN, J., ELLIS, C., MOHRIG, D.C., SWENSON, J.B., PARKER, G., HICKSON, T., HELLER, P.L., PRATSON, L., AND SYVITSKI, J., 2001, Experimental stratigraphy: *Geological Society of America, GSA Today*, v. 11, p. 4–9.
- PAOLA, C., TWILLEY, R.R., EDMONDS, D.A., KIM, W., MOHRIG, D., PARKER, G., VIPARELLI, E., AND VOLLER, V.R., 2011, Natural processes in delta restoration: application to the Mississippi Delta: *Annual Review of Marine Science*, v. 3, p. 67–91.
- PARTHENIADES, E., 1965, Erosion and deposition of cohesive soils: *American Society of Civil Engineers, Proceedings, Journal of the Hydraulics Division*, v. 9, HY1, p. 105–139.
- POSTMA, G., 1990, Depositional architecture and facies of river and fan deltas: a synthesis, *in* Colella, A., and Prior, D.B., eds., *Coarse-Grained Deltas: International Association of Sedimentologists, Special Publication 10*, p. 13–27.
- PRATSON, L., SWENSON, J., KETTNER, A., FEDELE, J., POSTMA, G., NIEDORODA, A., FRIEDRICH, C., SYVITSKI, J., PAOLA, C., AND STECKLER, M., 2004, Modeling continental shelf formation in the Adriatic Sea and elsewhere: *Oceanography*, v. 17, p. 118–131.
- PROTHERO, D.R., AND SCHWAB, F., 2004, *Sedimentary Geology: an Introduction to Sedimentary Rocks and Stratigraphy, Second Edition*: New York, W.H. Freeman and Company, 557 p.
- RANASINGHE, R., SWINKELS, C., LUIJENDIJK, A., ROELVINK, D., BOSBOOM, J., STIVE, M., AND WALSTRA, D., 2011, Morphodynamic upscaling with the MORFAC approach: dependencies and sensitivities: *Coastal Engineering*, v. 58, p. 806–811.
- RODRIGUEZ, A., HAMILTON, M., AND ANDERSON, J., 2000, Facies and evolution of the modern Brazos Delta, Texas: wave versus flood influence: *Journal of Sedimentary Research*, v. 70, p. 283–295.
- ROWLAND, J.C., DIETRICH, W.E., AND STACEY, M.T., 2010, Morphodynamics of subaqueous levee formation: insights into river mouth morphologies arising from experiments: *Journal of Geophysical Research-Earth Surface*, v. 115, F04007.
- RYER, T.A., 1981, Deltaic coals of Ferron Sandstone Member of Mancos Shale: predictive model for Cretaceous coal-bearing strata of Western Interior: *American Association of Petroleum Geologists, Bulletin*, v. 65, p. 2323–2340.
- RYER, T.A., AND ANDERSON, P.B., 2004, Facies of the Ferron Sandstone, east-central Utah, *in* Chidsey, T.C., Jr., Adams, R.D., and Morris, T.H., eds., *Regional to Wellbore Analog for Fluvial-Deltaic Reservoir Modeling: the Ferron Sandstone of Utah*: *American Association of Petroleum Geologists, Studies in Geology* 50, p. 59–78.
- SAMBROOK SMITH, G.H., BEST, J.L., ORFEO, O., VARDY, M.E., AND ZINGER, J.A., 2013, Decimeter-scale *in situ* mapping of modern cross-bedded dune deposits using parametric echo sounding: a new method for linking river processes and their deposits: *Geophysical Research Letters*, v. 40, p. 3883–3887.
- SHAW, J.B., WOLINSKY, M., PAOLA, C., AND VOLLER, V.R., 2008, An image-based method for shoreline mapping on complex coasts: *Geophysical Research Letters*, v. 35, L12405.
- SHAW, J.B., MOHRIG, D., AND WHITMAN, S.K., 2013, The morphology and evolution of channels on the Wax Lake Delta, Louisiana, USA: *Journal of Geophysical Research: Earth Surface*, v. 118, p. 1562–1584.
- SORIA, J.M., FERNÁNDEZ, J., GARCÍA, F., AND VISERAS, C., 2003, Correlative lowstand deltaic and shelf systems in the Guadix Basin (late Miocene, Betic Cordillera, Spain): the stratigraphic record of forced and normal regressions: *Journal of Sedimentary Research*, v. 73, p. 912–925.
- SYVITSKI, J.P.M., 2006, The morphodynamics of deltas and their distributary channels, *in* Parker, G., and García, M., eds., *River, Coastal and Estuarine Morphodynamics*: London, Taylor & Francis Group, p. 143–150.
- SYVITSKI, J.P.M., 2008, Deltas at risk: *Sustainability Science*, v. 3, p. 23–32.
- SYVITSKI, J.P.M., AND SAITO, Y., 2007, Morphodynamics of deltas under the influence of humans: *Global and Planetary Change*, v. 57, p. 261–282.
- THOMPSON, S., OSSIAN, C., AND SCOTT, A., 1986, Lithofacies, inferred processes, and log response characteristics of shelf and shoreface sandstones, Ferron Sandstone, central Utah, *in* Moslow, T.F., and Rhodes, E.G., eds., *Modern and Ancient Shelf Clastics: a Core Workshop: SEPM, Core Workshop 9*, p. 325–362.
- UITTENBOGAARD, R.E., AND VAN VOSSEN, B., 2004, Subgrid-scale model for quasi-2D turbulence in shallow water, *in* Jirka, G.H., and Uijtewaal, W.S.J., eds., *Shallow flows: Leiden, Balkema*, p. 575–582.
- VAN RIJN, L.C., 1993, *Principles of Sediment Transport in Rivers, Estuaries and Coastal seas*: Amsterdam, Aqua Publications, 614 p.
- VILKS, G., AND MUDIE, P.J., 1983, Evidence for postglacial paleoceanographic and paleoclimatic changes in Lake Melville, Labrador, Canada: *Arctic and Alpine Research*, v. 15, p. 307–319.
- VILKS, G., DEONARINE, B., AND WINTERS, G., 1987, Late quaternary marine geology of Lake Melville, Labrador: *Energy, Mines and Resources Canada, Geological Survey of Canada, Paper 87*, p. 22–50.
- WUNDERLICH, J., AND MULLER, S., 2003, High-resolution subbottom profiling using parametric acoustics: *International Ocean Systems*, v. 7, p. 6–11.
- WARDLE, R.J., AND ASH, C., 1986, *Geology of the Goose Bay–Goose River area*, *in* Current Research, Newfoundland Department of Mines and Energy, Mineral Development Division, Report 86-1, p. 113–122.
- WOLINSKY, M.A., EDMONDS, D.A., MARTIN, J., AND PAOLA, C., 2010, Delta allometry: growth laws for river deltas: *Geophysical Research Letters*, v. 37, L21403.
- ZENG, X., MCMEECHAN, G.A., BHATTACHARYA, J.P., AIKEN, C.L.V., XU, X., HAMMON, W.S., III, AND CORBEANU, R.M., 2004, 3D imaging of a reservoir analogue in point bar deposits in the Ferron Sandstone, Utah using ground-penetrating radar: *Geophysical Prospecting*, v. 52, p. 151–163.
- ZINKE, P., OLSEN, N.R.B., AND BOGEN, J., 2011, Three-dimensional numerical modelling of levee deposits in a Scandinavian freshwater delta: *Geomorphology*, v. 129, p. 320–333.

Received 27 August 2014; accepted 4 March 2015.